# Design of crotoxin-based peptides with potentiator activity targeting the ΔF508NBD1 Cystic Fibrosis Transmembrane Conductance Regulator

Marc Ravatin, Norbert Odolczyk, Nathalie Servel, J. Iñaki Guijarro, Eric Tagat, Benoit Chevalier, Nesrine Baatallah, Pierre-Jean Corringer, Gergely Lukács, Aleksander Edelman, et al.

Version of Record: https://www.sciencedirect.com/science/article/pii/S0022283622005563
Manuscript_4c78eb3bb2a9414b48a2d37a92805fb6

# Design of crotoxin-based peptides with potentiator activity targeting the ΔF508NBD1 Cystic Fibrosis Transmembrane Conductance Regulator

**Marc Ravatin[1,2,§], Norbert Odolczyk[1,3,4,§], Nathalie Servel[5], J. Iñaki Guijarro[6], Eric Tagat[2], Benoit Chevalier[5], Nesrine Baatallah[5], Pierre-Jean Corringer[1], Gergely L. Lukács[7], Aleksander Edelman[5], Piotr Zielenkiewicz[3,4], Jean-Marie Chambard[2,], Alexandre Hinzpeter[5,*], Grazyna Faure[1,*]**

[1]*Institut Pasteur, Université de Paris Cité, CNRS UMR 3571, Récepteurs-Canaux, Département de Neuroscience, 25, rue du Dr. Roux F-75015, Paris, France*

[2]*Sanofi, R&D, Integrated Drug Discovery, In Vitro Biology, Vitry-sur-Seine, France*

[3]*Department of Systems Biology, Institute of Experimental Plant Biology and Biotechnology, University of Warsaw, Miecznikowa 1, 02-096, Warsaw, Poland*

[4]*Institute of Biochemistry and Biophysics, Polish Academy of Sciences, Pawinskiego 5a, 02-106, Warsaw, Poland*

[5]*INSERM, U1151, Université de Paris Cité, Institut Necker Enfants Malades (INEM), CNRS, UMR 8253, 160 rue de Vaugirard, F-75015, Paris, France*

[6]*Institut Pasteur, Université de Paris Cité, CNRS UMR 3528, Biological NMR and HDX-MS Technological Platform, 28 rue du Dr. Roux F-75015, Paris, France*

[7]*Department of Physiology and Biochemistry, McGill University, Montréal, Quebec, Canada*

** Corresponding authors:*

*grazyna.faure-kuzminska@pasteur.fr; grazynafaure@gmail.com*

*alexandre.hinzpeter@inserm.fr*

§ 1st authors

## Abstract

We have previously shown that the CBb subunit of crotoxin, a β-neurotoxin with phospholipase $A_2$ ($PLA_2$) activity, targets the human ΔF508CFTR chloride channel implicated in cystic fibrosis (CF). By direct binding to the nucleotide binding domain 1 (NBD1) of ΔF508CFTR, this neurotoxic $PLA_2$ acts as a potentiator increasing chloride channel current and corrects the trafficking defect of misfolded ΔF508CFTR inside the cell.

Here, for a therapeutics development of new anti-cystic fibrosis agents, we use a structure-based *in silico* approach to design peptides mimicking the CBb-ΔF508NBD1 interface. Combining biophysical and electrophysiological methods, we identify several peptides that interact with the ΔF508NBD1 domain and reveal their effects as potentiators on phosphorylated ΔF508CFTR. Moreover, protein-peptide interactions and electrophysiological studies allowed us to identify key residues of ΔF508NBD1 governing the interactions with the novel potentiators. The designed peptides bind to the same region as CBb phospholipase $A_2$ on ΔF508NBD1 and potentiate chloride channel activity. Certain peptides also show an additive effect towards the clinically approved VX-770 potentiator. The identified CF therapeutics peptides represent a novel class of CFTR potentiators and illustrate a strategy leading to reproducing the effect of specific protein-protein interactions.

**Keywords: peptide design, protein-protein interaction, chloride channel potentiator, cystic fibrosis therapeutics peptides, phospholipase $A_2$**

## Abbreviations

AIRs: ambiguous interaction restraints

CF: cystic fibrosis

CFTR: cystic fibrosis transmembrane conductance regulator

ΔF508CFTR: the deletion of Phe508 in CFTR

CBb: isoforms of the basic subunit of crotoxin (β-neurotoxin from *Crotalus durissus terrificus* venom, made of CA and CB subunits)

cryoEM: cryo-electron microscopy

IBMX: 3-isobutyl-1-methylxanthine

ICL: intracellular loop

$K_D^{app}$ : apparent dissociation constant

MSD: membrane spanning domain

NBD: nucleotide binding domain

R domain: regulatory domain

TMD: transmembrane domain

aPC : automated patch clamp

RU: resonance units

STD: saturation transfer difference

$PLA_2$: phospholipase $A_2$ enzyme (EC 3. 1. 1. 4)

SPR: surface plasmon resonance

## Introduction

Cystic fibrosis (CF) is an inherited, multiorgan, life-shortening human disease with an autosomal recessive transmission. The *CF Transmembrane Conductance Regulator* (*CFTR)* gene was first identified in 1989 [1] in which more than 2000 genetic sequence variations have been identified, and near 400 correlating with CF pathophysiology [1–5].

These mutations mostly impact the structural integrity and function of the encoded CFTR protein, as well as its expression in epithelial cells [6]. Generally, mutations have a frequency of onset close to 0.1%, with a few exceptions such as the deletion three base-pairs of nucleotides encoding phenylalanine at position 508 (ΔF508) of the CFTR protein, which is by far the most common mutation expressed in CF patients with a frequency of 70% [7]. Dysfunction of CFTR caused by mutations has an impact on the regulation of fluid transport, resulting in chronic and progressive failure of several organs until death which occurs mainly as a result of respiratory, pancreatic or hepatic failure [6,8,9].

CFTR, a 1480-amino acid residue protein, belongs to the superfamily of ATP-Binding Cassette (ABC) transporters [1] and is the only member known to function as an ion channel [10]. It enables plasma membrane crossing of chloride and bicarbonate ions [11–13].

The 3D structure of the full-length CFTR protein was recently solved by cryo-electron microscopy (cryoEM) [14,15]. The structure shows that CFTR consists of two transmembrane domains (TMDs) forming a pore, two nucleotide binding domains (NBDs) controlling channel opening by ATP binding, and a single regulatory (R) domain [16] that plays an important role in CFTR activity regulation. Phosphorylation of the latter R domain by the cyclic AMP-dependent protein kinase A (PKA) is indeed crucial for channel gating [17,18].

The most severe mutations affect (I) protein synthesis (*e.g.* premature termination codons), (II) protein folding (*e.g.* ΔF508), and (III) channel gating (*e.g.* G551D). The deletion of F508 (ΔF508) in the NBD1 domain leads to defective folding, trafficking, and channel

gating at the plasma membrane. Only 1% of mutated CFTR (ΔF508CFTR) proteins reach the plasma membrane leading to significantly reduced chloride conductance [19].

Since the first discovery of the relationship between mutations in the *CFTR* gene and CF disease phenotypes, there has been an incessant endeavor to develop pharmacological approaches to correct the dysfunctions of the mutated CFTR protein [20]. Modulators that increase the open probability ($P_o$) of the CFTR channel are referred to as potentiators [21,22]. These molecules exert a potentiating effect on the activity of the CFTR channel by modifying the opening and closing cycle of the channel and therefore increasing the chloride ion current passing through the plasma membrane. In recent years, the development of the potentiator VX-770 (ivacaftor, Kalydeco®) [23] constituted an important breakthrough in the treatment of CF patients carrying mutations affecting channel gating [24]. Nowadays, around 5% of CF patients are treated with Kalydeco®. Potentiators are also used in association with CFTR correctors, *i.e.* molecules favoring the proper folding of ΔF508CFTR [25]. These molecules enhance maturation leading to higher levels of the channel at the cell surface.

While combinations of VX-770 with correctors such as VX-809 (Orkambi®) [26,27] or VX-661 (Symdeko®) [28,29] showed only modest clinical effects, the recently described triple combination VX-661/VX-445/VX-770 (Trikafta®) led to significant clinical benefits [30]. These results revealed that mutated CFTR could be targeted using a combination of small molecules, each alleviating a specific defect. Novel potentiators [31] or potentiators showing additive effects with VX-770 [32,33] are currently being developed to enhance the rescue of channels carrying gating mutations. Correctors with higher affinity [34] or novel corrector combinations and the addition of amplifiers to enhance protein expression are also in development (AbbVie, Proteostasis Therapeutics).

We recently showed that the CB subunit of crotoxin (CBb), a neurotoxin from *Crotalus durissus terrificus* venom [35], is a high-affinity binder of CFTR and ΔF508CFTR

[36]. CBb interacts with the nucleotide binding domain 1 (NBD1) of CFTR with nanomolar affinity, exhibiting both potentiation of chloride channel current of CFTR at the surface of epithelial cells and correction of misfolded ΔF508CFTR inside the cell [36]. We elaborated a structural model of the CBb-ΔF508CFTR complex by molecular modeling and validated it using biophysical methods, giving insights into the underlying mechanism by which CBb favors trafficking and activity of the abnormally folded CFTR channel [36].

The potentiating and correcting effects of CBb on ΔF508CFTR provide an original perspective to develop new molecules that could improve the two major defects associated with the ΔF508 mutation. CB (as well as its 4 natural isoforms $CBa_2$, CBb, CBc, CBd) is a neurotoxic phospholipase $A_2$ with seven disulfide bonds [37,38]. Its neurotoxicity, added to the difficulties of its expression, make it unsuitable for clinical or industrial use.

In this work, we hypothesized that an alternative to the use of CBb for therapeutics development was the design and use of peptides derived from CBb. The previously identified interaction interface of CBb with ΔF508NBD1 was used as a template for the development of new anti-CF agents. In this endeavor, we sought to identify the minimal region(s) of CBb associated with ΔF508CFTR potentiation, designed *in silico* several CBb-based peptides, and evaluated the peptides using biophysical and functional electrophysiology assays (manual and automated patch-clamp experiments).

Our results identified ten CBb-derived peptides that target ΔF508NBD1 and revealed their effects as potentiators on phosphorylated ΔF508CFTR. Moreover, we identified by NMR crucial residues of the peptides for ΔF508NBD1 binding, and together with an *in silico* approach, supported by mutational experiments, established the region of ΔF508NBD1 governing the interactions with novel potentiators. These CBb-derived peptides appear as excellent starting candidates mimicking the CBb potentiating activity of ΔF508CFTR, and we hope open a novel and promising strategy for future CF treatment.

## Results

For the rational development of new anti-CF agents, we followed a template-based modeling approach to propose peptides that mimic the CBb interface interacting with ΔF508NBD1 as defined by Faure et *al.* [36]. We designed three series of peptides: peptides derived from different continuous CBb interacting regions (Series I); peptides from different continuous CBb regions linked by a disulfide bridge (Series II), and *de novo* peptides designed to adopt a structure enabling the positioning of key residues implicated in the CBb-ΔF508NBD1 interactions (Series III).

### Design and functional characterization of Series I peptides

Series I ΔF508NBD1 peptide ligands were designed by *in silico* analysis of the previously proposed CBb-ΔF508NBD1 complex model (**Figure 1a**) using the COCOMAPS (bioCOmplexesCOntact MAPS) server [39] to identify protein-protein contacts, based on distance criteria (**Figures 1b** and **S1**). On the basis of the contact map with a cut-off distance set to 8 Å, three continuous sequence fragments of CBb were selected as initial fragments of peptide templates: (A) 1-HLLQFNKMIKFETRKN-16, (B) 16-NAVPFYAFYGCYCGWGGQ-33, and (C)105-NGYMFYPDS-113 (**Figure 1c**).

Templates A and C Series I peptides with different lengths and positions were studied to identify the shortest peptides able to bind to mutated NBD1 and potentiate the ΔF508CFTR channel. We evaluated the following peptides: A (1-HLLQFNKMIKFETRKN-16), A1 (1-HLLQFNKMIK-10), A2 (1-HLLQFNK-7) and C (105- NGYMFYPDS-113), C1 (107-YMFYPDSR-114), C2 (108-MFYPDSR-114) (**Figure 1c**). In the case of template B, which consists mainly of hydrophobic residues, we tested the original sequence B (16-NAVPFYAFYGCYCGWGGQ-33), and modified sequences designed to improve water solubility. The modifications were introduced on residues that do not interact with NBD1 in

the complex model:Y27D for peptide B1, Y27S for peptide B2, as well as Y21S, Y24S and C28S, for both peptides (**Figure 1c**). As negative controls in biological assays, we considered scrambled peptides with permutations of the original sequence of peptides A2 ($A2_{scr}$: FKHLLNQ) and C ($C_{scr}$: PSYDFNYMG).

## Direct binding of Series I peptides (A2, B and C) to ΔF508NBD1 of CFTR

Binding of peptides A2, B and C was evaluated by surface plasmon resonance (SPR), performed with recombinant human ΔF508NBD1 covalently attached to a CM-5 sensor chip. As shown in **Figure 2**, peptides A2, B and C directly interacted with immobilized ΔF508NBD1. The kinetic parameters of these interactions were determined by fitting the experimental association and dissociation curves to a 1/1 Langmuir binding model. The resulting apparent dissociation constants ($K_D^{app}$) were 26 ± 3 µM for peptide A2, 53 ± 9 µM for peptide B and 49 ± 6 µM for peptide C. The interaction, with peptide A2 and C appears to be specific and depends on the sequence rather than solely on the physicochemical characteristics of the peptides (hydrophobicity, charge), since control scrambled peptides containing a randomized sequence comprising the amino acid residues of A2 ($A2_{scr}$: FKHLLNQ) and C ($C_{scr}$: PSYDFNYMG) did not bind to ΔF508NBD1 (**Figure 2** and **S2**). As peptides A2, B and C directly bind to ΔF508NBD1, we hypothesized that Series I peptides could also modulate ΔF508CFTR $Cl^-$ channel activity.

## Potentiating effect of Series I peptides

In order to test large sets of newly synthetized peptides, the use of the electrophysiological automated patch-clamp (aPC) system QPatch (Sophion Biosciences) was a breakthrough combining high throughput and data robustness. This fully automated platform replicates the

sequence of events involved in manual patch-clamp. The required steps are cell positioning, cell sealing, cell clamping, and cell recording. The QPatch is an electrophysiological plate-based assay which allows to record up to 48 channels/cells in parallel in the whole-cell configuration. During this process, the cells are bathing in the external buffer, and following rupture of the plasma membrane the intracellular buffer, placed under the plate, fills the cells. Using this technique, Series I peptides were evaluated (**Tables 1** and **S1**). As the intracellular buffer cannot be changed during the experiment, and peptides were designed to bind to the intracellular ΔF508NBD1 domain, these had to be added to the intracellular solution. Hence, this QPatch protocol focused on the potentiating power of peptides without taking into consideration the cell penetrating potential of the peptides (see Materials and Methods). CBb was used as a reference (**Figure 3a**). In the presence of a forskolin-IBMX cocktail that activates the CFTR channel via PKA kinase, CBb exerted a potentiating effect on the activity of ΔF508CFTR at 1 and 10 nM. Under these conditions, CBb exhibited also an additive effect relative to the potentiator compound VX-770 (**Figure 3a**).

As shown in **Table 1** and **Figure 3b**, peptides A2 and B at 50 µM concentration exhibited a potentiating effect on the phosphorylated channel, without additivity to VX-770. Peptides C and C2 exerted a potentiating effect on the phosphorylated ΔF508CFTR channel at 5 µM as well as an additive effect to VX-770 at 50 µM, similarly to CBb (**Figure 3a, Table 1**). Peptides A (50 µM) and C1 (5 µM) were active only in the presence of VX-770 ( **Table 1**). Peptides A1, B1 and B2 as well as control peptides $A2_{scr}$ and $C_{scr}$ were found to be inactive (**Table S1**).

The activity of peptides A2, B and C was also tested by whole-cell manual patch-clamp. Peptides were applied from the outside on HeLa or HEK293 cells stably expressing ΔF508CFTR.. To enable ΔF508CFTR cell surface expression, cells were pre-treated 24h with corrector c407 (10 µM) as previously performed for CBb [36] and illustrated on **Figure S3A**.

Patch-clamp recordings showed that under these conditions, peptides A2 and C were not active (**Figure S3A**), while peptide B potentiated ΔF508CFTR (**Figure 4a-c** and **Table S2**). The lack of activity of the hydrophilic peptides A2 and C, in apparent contrast with QPatch results, could be due to an internalization problem, as it is known that hydrophilic peptides generally cannot cross the membrane. We thus performed internalization experiments of FITC-labeled peptide C, either "naked" or with liposomes to facilitate membrane translocation. As the results clearly indicated that liposomes were required for efficient internalization of this hydrophilic peptide into HeLa cells (**Figure S3B)**, we repeated the patch-clamp experiment with peptides A2 and C coated with liposomes. In the presence of liposomes, both peptides showed a significant potentiating effect (**Figure 4a-c** and **Table S2**), consistent with QPatch experiments. The application of liposomes alone had no effect on CFTR current (**Figure S3A**). The A2+C combination (1 µM each) was found to potentiate ΔF508CFTR current (**Figure 4a-c** and **Table S2**), but without increasing the potentiating effect of either A2 or C alone.

## Design of disulfide-bonded peptides (Series II) and demonstration of the potentiating effect of peptide N3

To verify whether covering a larger part of the interaction interface could improve the potentiating activity of peptides, we decided to design peptides (Series II, named N) composed of a fragment of peptide C2 (extended by a cysteine at position 115) and different fragments of template B (**Figure 5**) connected by a disulfide bridge, which naturally occurs in the CBb protein between C26 and C115 [35]. The peptides N1 (22-AFYGC-26 + 109-FYPDSRC-115), N2 (26-CYSGWGGQ-33 + 109-FYPDSRC-115) and N3 (16-NAVPFSAFSGCDSGWGGQ-33+ 108-MFYPDSRC-115) were synthesized and tested by QPatch. Whereas, peptides N1 and N2 had no influence on ΔF508CFTR channel activity

(**Table S1**), peptide N3 acted as a potentiator of the phosphorylated channel and displayed additivity with VX-770 (**Figure 6** and **Table 1**). Interestingly, within Series II, the only active peptide (N3) contains three aromatic residues: F23, W30 and F109 (**Figure 5**), which in the complex model are located on the central part of the CBb interface (**Figure 7a**). This observation suggested that these residues could be important for the interactions with ΔF508NBD1 and might be responsible for the potentiating activity of the peptides.

## Design of Series III peptides and demonstration of the potentiating effect of peptides M2, M3 and M10

We noticed that the spatial arrangement of F109, F23 and W30 corresponds with an arrangement of n, n+4 and n+8 residues in an α-helix (**Figure 7b-d**). We hence hypothesized that peptides with an α-helical structure containing the motif FxxxFxxxW may mimic the central part of the CBb interface, interact with ΔF508NBD1 and potentiate its activity. To test this hypothesis, we searched the motif FxxxFxxxW in the PDB database using PROSITE (https://prosite.expasy.org/), extracted the atomic coordinates of α-helical regions containing the motif and superimposed the peptide structures on the CBb-ΔF508NBD1 complex model using CBb residues F109, F23 and W30 as reference. After visual assessment, ten sequences were selected (Series III peptides, named M), synthesized and subjected to experimental evaluation (**Tables 1**, **S1** and **S3**). Additional mutations were introduced to some of the selected sequences to increase their solubility. Automated patch-clamp experiments showed that peptides M2, M3 and M10 were able to mimic CBb acting as potentiators and also displaying additive effects with VX-770 (**Tables 1**, **S1** and **Figure 8**). Finally, we compared all active peptides from the three Series with CBb and evaluated their activities by statistical

analysis (ANOVA). The Series III peptides M2, M3 and M10 were found to be the most active, with comparable potentiating and additive effects (**Figures S4A and S4B**).

## NMR STD characterization of Series III peptides M10 and M4

In order to establish the importance of the peptide residues for the interaction, we determined the atoms of Series III peptides that are in close contact with ΔF508NBD1 using $^{1}$H-detected ligand-observed NMR STD (saturation transfer difference) experiments. We focused on M10, which exhibited the best potentiating and additive effects across the three Series and selected peptide M4 as a control, as it did not display any functional effect in electrophysiology assays but contains the FxxxFxxxW motif (**Figures S4A and S4B, Tables S1** and **S3**). In STD experiments, only the signals of the peptide atoms in close contact with the protein are observed. As both peptides M4 and M10 showed residual STD signals in control experiments in the absence of the protein, we corrected the STD (cSTD) values using the difference between the STD values in the presence and absence of ΔF508NBD1 (see Materials and Methods for details). The peptide resonances were assigned to their corresponding $^{1}$H atoms using standard procedures (**Tables S4** and **S5**). Interestingly, although M10 is active and M4 is inactive, both peptides were found to interact with the NDB1 domain. As can be observed in **Figure 9a**, which displays the aromatic (~6.5-8 ppm) and amide (~8.6-8.0 ppm) $^{1}$H region of the reference (black) and cSTD spectra (blue), most of the aromatic protons and only a few of the amide protons of peptides M4 and M10 show a cSTD signal, indicating that the aromatic rings of both peptides are involved in the interaction with ΔF508NBD1. The determined values of cSTD are reported in **Table S6** and schematized with color coded spheres on the chemical structure of the peptides in **Figure 9b**. Of note, the intensity of the cSTD signal depends on the distance to the protein atoms, the number of protein atoms in

contact and the residence time within the complex. Its magnitude can thus be compared for different atoms within a ligand but is difficult to compare quantitatively for different ligands with different residence times without knowing the structure of the complex. Several features can be inferred from the cSTD of both peptides: (I) the aromatics rings of F and W residues in the FxxxFxxxW motif are important for the interaction, in agreement with the peptide design hypothesis, (II) the C-terminal W residue shows the highest number of contacts and very high cSTD values, indicating its crucial role, (III) except K3 in peptide M4, positively charged residues are important, while (IV) negatively charged residues and small polar (N, S, T) or non-polar (A) do not interact, (V) additional F aromatic rings establish contacts with the protein, and (VI) both peptides make extensive contacts with ΔF508NBD1.

## The double mutant ΔF508-Y625A CFTR is resistant to peptide M2 potentiation

To test the validity of the model at the origin of the peptide design, pinpoint the peptide binding site and establish the importance of aromatic amino acid residues of NBD1 suggested by the CBb-ΔF508NBD1 complex model, in particular Y625, F626, Y627 (see **Figure 1a**, bottom left panel), we mutated these residues into alanine, alone and in combination with ΔF508. The effect of these mutations was first evaluated on CFTR maturation itself in transiently transfected HEK293 cells. Western blot analysis of WT-CFTR showed a normal maturation profile *i.e.* two bands, a mature fully-glycosylated CFTR band at 170 kDa (band C), and a core-glycosylated CFTR band at 150 kDa (band B). Single point mutations F626A and Y627A disrupted proper CFTR maturation, while Y625A did not (**Figure S5A**).

To evaluate the implication of Y625 in peptide binding, we performed manual whole-cell patch-clamp with the ΔF508 and ΔF508-Y625A CFTR mutants in transiently transfected HEK293 cells. We chose to work with the peptide M2 (in the presence of liposomes to favor internalization) – as this peptide showed an activity (**Figure 8**). To enable expression of mutant proteins at the cell surface, cells were corrected at 27°C for 4-16h prior to patch-clamp

experiments. The results confirmed a significant potentiating effect on ΔF508CFTR of peptide M2, whereas the double mutant ΔF508-Y625A CFTR was resistant to M2 potentiation (**Figure 10, Table S7**), indicating that mutation of this single residue Y625 was sufficient to prevent potentiation. Of note, similar potentiation was achieved with VX-770 using mutants G551D CFTR and G551D-Y625A CFTR, indicating that Y625A did not prevent channel potentiation (**Figure S5B**). These results indicate that the aromatic cluster of ΔF508NBD1 implicated in the interaction with peptides according to the complex model is important for both channel folding (F626, Y627) and potentiation (Y625) by peptide M2. These results are also consistent with data from NMR cSTD experiments which highlighted the importance of the hydrophobic, aromatic peptide residues (in the motif FxxxFxxxW) for the interaction of series III peptides with ΔF508NBD1, which suggests binding to the hydrophobic region of the protein. Together, these findings support that peptide M2 binds to the region predicted by the CBb-ΔF5080NBD1 structural model and highlight the importance of residue Y625 for the direct interaction with the M series peptides.

## Peptide M10-ΔF508NBD1 complex model generated by molecular docking

To predict the possible binding mode of M series peptides, we performed molecular docking simulations between ΔF508NBD1 and peptide M10, the best potentiator from Series III, using the docking software HADDOCK (High Ambiguity-Driven protein-protein DOCKing) [40,41]. HADDOCK is a flexible docking approach that includes constraints from predicted or identified protein interfaces with ambiguous interaction restraints (AIRs) to drive the docking procedure. As our model of CBb and ΔF508NBD1 complex structure [36] was in agreement with experimental HDX-MS (Hydrogen-Deuterium eXchange followed by Mass Spectrometry) data [36], and Y625 was proven to be important for M2 potentiation, we assumed that the interaction interface of ΔF508NBD1 with peptide M10 should reside on the

same surface observed for CBb. Thus, AIRs defined as "passive" were adopted from the CBb-ΔF508NBD1 model and Y625 was defined as an "active" residue. Peptide M10 was modelled as an α-helix. The AIRs for peptide M10 were based on experimental NMR data: residues defined as "strong" or "very strong" on the basis of cSTD values were defined as "active", whereas all other peptide residues were defined as "passive" (**Figure 9b**). The results for the best cluster (20 structures out of 99 final water-refined structures) are reported in **Table S8** and the corresponding representative structure of the M10-ΔF508NBD1 complex is shown on **Figure 11**. The model is fully consistent with NMR data where (i) all three hydrophobic residues of motif FxxxFxxxW from peptide M10 are involved in the interactions with ΔF508NBD1, the peptide residues F1 and F5 create hydrophobic interactions with Y625, F669 of ΔF508NBD1, whereas W9, which was shown by NMR as crucial for interaction, is in proximity to residues F626 and Y627 of the protein. (ii) The positively charged R2 seems to be important as its side chain may create an ionic interaction with E621, be a hydrogen bond donor to Y625 (side chain-side chain interaction) or to F669 (main chain-main chain interaction), while (iii) all negatively charged peptide residues do not interact with the protein. However, E6 could stabilize the orientation of R2 to interact with E621.

## Discussion

The treatment of CF patients has significantly improved with the identification of CFTR modulators, small molecules that bind directly to the protein, either promoting its proper folding (correctors) or enhancing chloride channel activity (potentiators). As these compounds were identified using high-throughput screens [42–44], their specific binding sites and mechanism of action were not precisely determined until recently.

The CFTR correctors VX-809 (or its derivative VX-661) and VX-445 were shown to bind to the Membrane-Spanning Domain 1 (MSD1) and to Nucleotide Binding Domain 1 (NBD1) [45–49], while potentiator VX-770 was shown to bind to MSD1 [50]. Although small molecules have been developed for nearly two decades, the peptide-based approach is quite novel in the field [51], in particular for peptides that may directly bind to ΔF508CFTR and act as modulators (potentiators/correctors). Until recently, only the Esc peptides had been identified as direct binders of ΔF508CFTR, and their ability to potentiate CFTR related current was reported by Ferrera and co-workers [52].

The strategy developed in this study differs from previous methods and is based on a structure-template-based modeling approach to design peptides that mimic the CBb-binding interface with ΔF508NBD1. With this methodology, we identified ten peptides with a potentiating effect on ΔF508CFTR channel chloride current: peptides A, A2, B, C, C1, C2 (Series I); peptide N3 (Series II) and peptides M2, M3, M10 (Series III). The peptides with a hydrophobic FxxxFxxxW motif (Series III) appeared as the most active potentiators and open an original approach to develop short peptide-based modulators of ΔF508CFTR. Moreover, this strategy could be extended and applied to other systems for which the structures of the binding partners are available.

The key residues of the peptide M10 involved in ΔF508NBD1 binding were identified experimentally identified, their importance was determined by NMR, and were further utilized as constraints to propose a M10-ΔF508NBD1 complex structural model by molecular docking. Intriguingly, all the proposed peptides in Series III contain the hydrophobic motif, but only three of them are active as ΔF508CFTR potentiators. This could be, at least in part, related to different helical propensities and entropic penalties of the ordering of disordered peptides in solution to adopt an α-helical structure upon ΔF508CFTR binding. Such entropic penalties could be significantly overcome by preparing stapled peptides to stabilize α-helical

structures of the M series peptides and enhance their activity, which is now under investigation.

The electrophysiology experiments performed with the ΔF508-Y625ACFTR mutant supported our *in silico* findings that the protein residue Y625 may be crucial for M series peptides' binding. Indeed, the double mutated protein ΔF508-Y625ACFTR is resistant to potentiation by peptide M2, contrary to ΔF508-CFTR. This strongly suggests that Y625, together with other aromatic residues (F626, Y627) located nearby on the surface of NBD1, is involved in hydrophobic interactions with peptides from Series III that lead to their potentiating activity.

As both CBb and the identified potentiating peptides target ΔF508NBD1, we can postulate that potentiation occurs by favoring or stabilizing NBD1 dimerization. Other known CFTR potentiators enhance channel activity by favoring or stabilizing NBD dimerization, such as ATP analogues [53–59], genistein [60–62] and SBCs [63]. This is consistent with the additivity observed between several peptides and VX-770, indicative of distinct mechanisms of action. Enhanced channel potentiation could be of great interest to treat CF patients presenting suboptimal responses to VX-770 [33,64].

While the mechanism of action of these peptides needs further investigation, it is interesting to note that amino acids at the CBb-NBD1 binding interface, such as Y625 and Y627, can potentially be targeted by the tyrosine kinases Src and Pyk2, which were shown to activate CFTR [65]. This region therefore appears to be important in both the activation and potentiation of CFTR.

The strategy developed herein could also be applicable to other CFTR interacting partners and different regions of the chloride channel, such as the N-terminal loop of CFTR which interacts with WNK1. This protein-protein interaction was shown to modulate channel permeability independently of WNK1 kinase activity [66]. The developed strategy enabling

the design of peptides, as described here, could lead to discover new CFTR modulators favoring conformational changes affecting channel opening or selectivity.

## Materials and Methods

### Materials

ΔF508NBD1 was purified as described elsewhere [67]. Peptides (>95% purity) were produced and supplied in lyophilized form by ProteoGenix (Schiltigheim, France). Peptides were dissolved in milliQ water or in 100% acetonitrile and gradually diluted with milliQ water (depending on the degree of hydrophobicity) and stored at -20 °C. Upon dissolution, an amino acid composition analysis was systematically carried out in order to determine the concentration of the peptides in solution (Chemistry of Biomolecules Unit, Institut Pasteur).

### *In silico* design of peptides

*Peptides- Series I (A, B, C) and II (N)*

The model of the CB-ΔF508NBD1 complex was built and described previously [36]. The protein-protein interaction interface was defined according to the method implemented in the bioCOmplexesCOntact MAPS server (COCOMAPS: https://www.molnac.unisa.it/Bio-Tools/cocomaps/) [39]. The analysis of the protein-protein interfaces and selection of CBb fragments potentially suitable for modulator peptides were done on the basis of intermolecular contact maps created by COCOMAPS (the cut-off distance was set to 8 Å) and by visual inspection of the CBb-ΔF508NBD1 complex structure. Structure visualization, analysis and structural figures were done using PyMOL (Version 2.3.0, Schrödinger, LLC, New York, USA).

*Peptides- Series III (M)*

The PDB database (https://www.rcsb.org) [68] was scanned against the sequence motif "FxxxFxxxW" using the ScanProsite tool [69]. Hit structures were filtered by in-house python scripts to select for analysis only "FxxxFxxxW" motifs localized on α-helical structures. The selected protein fragments were superimposed (Cα atoms) with PyMOL to F23, W30, and F109 of CBb in the CBb-ΔF508NBD1 complex. After this procedure, the CB structure was removed and potential complexes of peptides-ΔF508NBD1 were analyzed by visual inspection.

## Peptide Docking

The α-helical structure of peptide M10 was extracted from the PDB structure (PDB ID: 6PSY), which had been previously selected by a Prosite search (see previous paragraph). Changes to the original sequence (491-FFKDFLTFW-499) were introduced in PyMOL. The ΔF508NBD1 structure (1XMJ) for peptide docking was derived from the complex CBb-ΔF508NBD1 model prepared previously [36]. The peptide M10 was docked on the HADDOCK2.4 web server, with the standard procedure, and optimized for peptide docking [40,70,71].

## Manual patch-clamp

HeLa cells stably expressing ΔF508CFTR [72] or transiently transfected HEK293 cells were seeded in 35-mm diameter petri dishes before being mounted on an inverted microscope. Cell lines used were: HEK293 ΔF508 for peptides A and M2. HeLa ΔF508 for peptides B, C and A2+C. Correction was obtained either by a pharmacological chaperone (1 µM c407) for peptides C or (A2+C), or by low temperature (27°C) for peptides A2 and B.

The patch-clamp experiments and whole-cell patch recordings were performed as previously described [73] and [36]. Briefly, ΔF508CFTR correction was achieved using corrector c407 (1 µM, 24h), or low temperature incubation (27°C, 16h). Potentiating effects were

independent of the correction method used. Whole cell patch-clamp recordings were performed at room temperature with an Axopatch 200B amplifier controlled by a computer via a Digidata 1550B interface (Axon Instruments, USA). The pipettes were drawn from borosilicated glass (Kimax 51) using a Sutter P-87 micropipette puller and the tips were flame polished. Recordings were made using the whole-cell patch-clamp configuration after perforating the membrane with nystatin. The stock of nystatin (N6261, Sigma) (50 mg/mL) was prepared daily in DMSO and the stock solution diluted (1:250) with the internal solution, sonicated for 1 min and 0.22 µm filtered (2.15 µM). The internal solution contained (in mM): 131 NaCl, 2 $MgCl_2$ and 10 HEPES-Na (pH 7.3), while the external solution contained (in mM): 150 NaCl, 1 $CaCl_2$, 1 $MgCl_2$, 35 sucrose and 10 HEPES-Na (pH 7.3). The currents were recorded by applying a steady potential jump of -60 mV for 1 s, with a holding potential of 0 mV and an interval of 3 s. To establish the current-voltage curves (I-V curve), a series of 9 potential jumps between −100 and +80 mV, of a duration of 1 s each, is carried out. The CFTR current is activated using 400 µM of cyclic 8-(4-chlorophenylthio-)AMP (CPT-AMPc, Sigma) and 100 µM of 3-isobutyl-1-methylxanthine (IBMX, Sigma).

When maximum stimulation is reached, a solution additionally containing 1 µM CBb-derived peptide is added to test the potentiation of the CFTR current. When this second maximum stimulation is reached, a solution additionally containing 5 µM of $inh_{172}$ (a CFTR inhibitor) and 20 µM glibenclamide is added to ensure the specificity of the current measured. CFTR currents are defined as the difference of the current recorded during maximal stimulation by the CPT-AMPc cocktail (or peptide cocktail) and the current measured after inhibition with the inhibitor cocktail. Data were analyzed using the nonparametric (paired samples) Sign test between cAMP-activated CFTR current and peptide-potentiated CFTR current. Significant potentiation by peptides was established if $p < 0.05$. The nonparametric (independent samples)

Mann-Whitney test was performed to compare two peptide treatments. A peptide treatment is defined to be significantly better if $p < 0.05$ for the CFTR current increase.

*Lipofection*

One to 5 nmol of peptide corresponding to 50 µl of 20 µM PBS-diluted peptide (1/250 µl of stock-solution at 5 mM) were mixed with 5µl of dried Pierce liposomes (film resuspended in 250 µl of methanol before aliquoting and drying), according to supplier's instructions (Pierce™ Protein Transfection Reagent, ThermoFisher). After 5 minutes of incubation, the final volume was brought to 500 µl with serum free medium (Optimem). Cells (70% confluency on cover slips) were washed with Optimem and the complex of peptides and liposomes was directly applied onto cells. Cells were incubated in a 5% $CO_2$ incubator at 37°C for times ranging from 15 minutes to 24 h. Cells were then rinsed with PBS, fixed with 4% paraformaldehyde for 15 minutes and rinsed with PBS. Cover slips were transferred on microscope slides mounted in Vectashield medium with Dapi, and covered with a new cover slip.

*Confocal microscopy*

Image acquisition was performed on a Leica TCS SP5 AOBS confocal microscope (63x/1.4 oil objective). Figures were created with an ImageJ plugins FigureJ [74].

## Automated patch-clamp (aPC, QPatch)

*Cell culture*

A stable FRT cell line expressing ΔF508CFTR (Sanofi Genzyme, Framingham, US) was used to conduct these experiments. Cells were cultured at 37°C in F-12 modified Coon's medium (F0855-BC from Merck) supplemented with 10% FBS (Life Technologies), Zeocin 400 µg/mL (Invivogen) and 1% L-glutamine (Gibco) in T75 flasks. For the ΔF508CFTR correction step, FRT cells were incubated with VX-809 (3 µM) 24 to 48h. Reaching a very

light confluence rate after 3-4 days (about 30-40%) has been chosen in our protocols to ensure the best rate of tested cells in APP protocols. Cells are detached with trypsin 1X 1mL for 5 minutes (Sigma) after being washed with PBS (Gibco™). Trypsin activity is stopped by one wash with Coon's medium and then two washes with specific culture medium without serum (EX-CELL® CD CHO Serum-Free Medium, ref.14361C, Merck).

*Solutions and chemicals*

Experiments were done with equal chloride concentrations in intra and extracellular buffers. Extracellular solution contains (in mM) NaCl 150, KCl 4, $CaCl_2$ 2, $MgCl_2$ 1, HEPES 10 (pH = 7.4, 320 mOsmol/kg) and intracellular solution contains (in mM) KCl 120, NaCl 5,$CaCl_2$ 5, $MgCl_2$ 1.75, EGTA 10, HEPES 10 and MgATP 4 (added just before use) (pH = 7.2, 290 mOsmol/Kg) (all chemical entities were purchased from Sigma). Slight modifications of the main ion entity allow us to adjust the osmolarity. Compound powders of $inh_{172}$ (Sigma, C2992), glibenclamide (Sigma, G0639), forskolin (Sigma, F6886), IBMX (Sigma, I5879) and VX-770 (from Biovision, Sigma, CalbioChem ref. 5305410001) are solubilized in DMSO (Sigma) and stocked at -20°C until thawing and dilution in extracellular solution just before use.

*aPC experiments and results analysis*

Electrophysiological screening tests were performed on a QPatch platform (Sophion Bioscience) using single- and multi-hole QPlates. CBb and peptide candidates must exert their biological activities by their ability to bind to the ΔF508NBD1 domain, which is located in the intracellular side of the cell. This property implies an exchange of the intracellular medium used by QPatch during the experiment without and with CBb and peptides during sealing/control whole-cell recording and compound addition steps, respectively. This is not feasible according to QPatch routine protocols, where tested molecules are usually directly applied in the extracellular medium. To adapt the protocols it was therefore needed to this

unconventional experimental needs: peptides being active on the intracellular side, each pipette had to be independent of each other. Hence, a pipette had to dispense intracellular fluid with a given peptide concentration on the QPlate (therefore a pipette of the QPatch dispenses defined intracellular medium for six tested cells). Boats were also adapted in the aim of having a maximum of eight intracellular buffers containing two concentrations of peptides to be tested per QPlate. Once these different intracellular solutions had been dispensed, extracellular solution with the appropriate cell density was applied to obtain successful seal and whole-cell steps. Then, phosphorylation of ΔF508CFTR channels was achieved by application of a cocktail of activators (e.g. forskolin 1 µM + IBMX 100 µM). The next solution to be applied was the same cocktail of activators with addition of 10 µM VX-770, which is the reference for potentiation of ΔF508CFTR. Finally, at the end of each cell recording, a mix of reference blockers (10 µM $inh_{172}$ + 100 µM glibenclamide) was applied to fully block the elicited currents and validate the specificity of the ΔF508CFTR recordings. From a holding potential of - 50 mV, currents were elicited using 2600 seconds voltage ramp protocols ranging from - 100 to + 100 mV. Current amplitudes were recorded at -80 and +80 mV. For each compound application, the last 20 recordings were used for the online analysis performed by the Analyzer Software (Sophion). All raw data, as well as the four steps of the assay, are illustrated in **Figure S6**. Data were first normalized using cell capacitance and then used to identify cells that deviated from the general trend. Indeed, cells which exhibited any of the following characteristics were discarded from the analysis process: insufficient resistance after obtaining the whole cell configuration (R < 200 MOhm), Rserie ≥ 10 MOhm, incomplete inhibition by reference compounds (< 50%), the capacitance < 10 pF or > 17 pF, data are illustrated by Tuckey boxes (**Figure S6**). Statistical analysis of variances were carried out using the standard Anova or

Anova type according to the results of the normality and Levene's tests carried out upstream (Everst@t 6.1.0, Sanofi).

## Surface plasmon resonance (SPR) binding studies

SPR experiments were performed at 20 °C using a Biacore 2000 system (Biacore AB, Cytiva Lifesciences). Recombinant ΔF508NBD1 was covalently coupled via primary amino groups on a CM5 sensor chip, as described (Faure *et al.,* 2016).The carboxymethylated dextran matrix was activated with 35 µl of an EDC/NHS (1/1) mixture. Ten µl of ΔF508NBD1 at a concentration of 20-40 µg/mL in 10 mM sodium acetate, pH 4.5 with 2 mM MgATP and 2 mM DTT were injected (to reach an amount of immobilized protein in the range 8k to 13k RU) and unreacted groups were blocked with 35 µl of ethanolamine (pH 8.5). The running buffer for the immobilization protocol was HBS-P (Cytiva Lifesciences), supplemented with 1 mM DTT and a flow rate for immobilization of 5µL/min. A separate flow channel on the same sensor chip, reserved for control runs, was subjected to a blank immobilization run by preparing it in the same way but without ΔF508NBD1.

For binding experiments between immobilized ΔF508NBD1 and peptides, running and sample buffer had the following composition: 50 mM Tris, 150 mM NaCl, 3 mM $MgCl_2$ (pH 7.5), 0.005% P20, 2 mM MgATP and 2 mM DTT (Sigma). The protein-peptide interaction was monitored at 15°C by injecting different peptide concentrations (50 to 600 µM and then adapted from the firsts results obtained to lowest concentrations), with a flow rate of 20 µL/min, and recording the refractive index changes at the sensor surface. The subsequent dissociation phase was followed after each association run by injecting the running buffer alone. Surfaces were regenerated by injection of 5 µL of 5 mM NaOH and 5 µl of 10 mM glycine-HCl (pH 1.5). All association and dissociation curves were corrected for non-specific binding by subtraction of control curves obtained from injection of the analyte concentrations through the blank flow channel. The apparent kinetic constants, $k_{on}$ and $k_{off}$, were calculated

using the Biacore BIAEVALUATION 4.1 software (Biacore AB, Cytiva Lifesciences), assuming a simple two-component model of interaction. Each run consisted of at least three independent measurements (three different immobilization flow paths and one control flow path)

## NMR Saturation Transfer Difference

For resonance assignment, peptide M4 and M10 samples (1 mM) were prepared in 20 mM deuterated (d11 98%, Eurisotop, St Aubin, France) Tris$D_{11}$Cl pH 7.6 150 mM NaCl 4% $D_2O$. For interaction studies and controls, peptides (1 mM) and peptide (1 mM): ΔF508NBD1 (30 µM) samples were prepared in the same buffer supplemented with 1 mM 3'-deoxy ATP (dATP), 1 mM TCEP [tris(2-carboxyethyl)phosphine] and 15 mM $MgCl_2$.

Experiments were performed using 800 MHz Avance Neo or 600 MHz Avance III HD (Bruker, Billerica, USA) spectrometers both equipped with a cryogenically cooled triple resonance $^{1}H[^{13}C/^{15}N]$ probe. Experiments are referenced relative to external DSS (sodium salt of 4,4-dimethyl-4-silapentane-1-sulfonic acid). Peptide resonances were assigned following standard procedures from homonuclear $^{1}H$-$^{1}H$ two-dimensional DQF-COSY (double quantum filtered correlation spectroscopy) [75], TOCSY (total correlation spectroscopy), NOESY (nuclear Overhauser enhancement spectroscopy) [76,77] and ROESY [78] spectra. Interactions were probed at 15 °C (800 MHz) using STD (saturation transfer difference) experiments. These experiments used 2 s selective (0.2 ppm) on-resonance (-0.5 ppm) and off-resonance (-40 ppm) saturation achieved with trains of adiabatic e-BURP2 pulses (excitation band-selective uniform-response pure-phase 2) [79,80]. STD data were recorded for samples of peptide in the presence of ΔF508NBD1, and of peptide-only under the same conditions. Some STD signal was observed for the peptide-only samples. To obtain the contribution of the ΔF508NBD1-peptide interaction to the observed STD signal, the STD spectra of the peptide-only spectra were subtracted from the protein:peptide STD spectra. The

corrected STD signal (cSTD) was calculated from the ratio of the integrals of a peak in the corrected STD spectrum and the corresponding reference (off-resonance) spectrum. Errors in cSTD values were determined from noise standard error integrated over an equivalent region.

### Plasmids and mutagenesis

The cDNA of CFTR WT (M470) subcloned in pTracer was mutated using the QuickChange XL II mutagenesis kit (Agilent) following the manufacturer's instructions. Obtained mutants were fully sequenced, amplified and purified (Macherey-Nagel). Plasmid concentrations were measured using a Nanodrop (Thermo Fisher Scientific).

### Western blot

HEK293 cells were cultivated in DMEM medium supplemented with 10% fetal calf serum (Thermo Fisher Scientific) and maintained at 37°C, 5% $CO_2$. Cells seeded in 6-well plates were transfected with CFTR WT and mutant plasmids using Lipofectamine 3000 (Thermo Fisher Scientific). After 24 hours, transfected cells were lysed in RIPA buffer containing protease inhibitors and the protein concentration was assessed using the RcDc assay (BioRad). Western blot analysis was performed using 60µg of protein from each sample separated on a 7% acrylamide gel. After transfer onto nitrocellulose membranes, CFTR was probed using antibody 660 (NACF Foundation) and α-tubulin was probed with antibody DM1A (Santa Cruz).

## Acknowledgments

We thank Dorothée Tamarelle for performing the automated patch-clamp biostatistical analysis (Sanofi, Non clinical biostatics Department, Vitry sur Seine, France). We thank S. Bayand and C. Ganneau for amino acid composition analysis (Chemistry of Biomolecules Unit, Institut Pasteur). We are grateful to Matthieu Cornet and Nicolas Goudin for performing

the manual patch-clamp statistical analysis (Statistical Data analysis and Imaging Necker Bioimage Analysis Platform).

## Conflict of interest

The authors declare that they have no conflict of interest.

## Author Contributions

Project Supervision: GF, JMC, AH. Conceived and designed the experiments: GF, MR, NO, JMC, AH, JIG, AE, PJC. *In* silico strategy and concept of peptides designed: NO, PZ. Performed *in silico* studies: NO. Performed the experiments: MR, NS, JIG, BC, NB. Analyzed the data: NO, MR, NS, ET, JIG, AH, JMC, GF. Provided the recombinant ΔF508NBD1: GLL. Wrote the paper: MR, NO, NS, JIG, JMC, AH, GF.

## Data Availability

The datasets generated and/or analyzed during the current study are available from the corresponding authors on reasonable request.

## Competing Interests

The authors have no relevant financial or non-financial interests to disclose.

## Funding

The research leading to these results has received partial funding from Vaincre La Mucoviscidose (VLM) grant N° RF20170502000/1/1/141; from contract SANOFI-Aventis

R&D/Institut Pasteur (grant n°199038). MR was a recipient of PhD-CIFR Fellowship from SANOFI-Aventis R&D. The 800-MHz NMR spectrometer of the Institut Pasteur was partially funded by the Région Ile de France (SESAME 2014 NMRCHR grant n° 4014526).

References


[1] J.R. Riordan, J.M. Rommens, B. Kerem, N. Alon, R. Rozmahel, Z. Grzelczak, J. Zielenski, S. Lok, N. Plavsic, J.L. Chou, Identification of the cystic fibrosis gene: cloning and characterization of complementary DNA, Science. 245 (1989) 1066–1073. https://doi.org/10.1126/science.2475911.

[2] C. Castellani, H. Cuppens, M. Macek, J.J. Cassiman, E. Kerem, P. Durie, E. Tullis, B.M. Assael, C. Bombieri, A. Brown, T. Casals, M. Claustres, G.R. Cutting, E. Dequeker, J. Dodge, I. Doull, P. Farrell, C. Ferec, E. Girodon, M. Johannesson, B. Kerem, M. Knowles, A. Munck, P.F. Pignatti, D. Radojkovic, P. Rizzotti, M. Schwarz, M. Stuhrmann, M. Tzetis, J. Zielenski, J.S. Elborn, Consensus on the use and interpretation of cystic fibrosis mutation analysis in clinical practice, J Cyst Fibros. 7 (2008) 179–196. https://doi.org/10.1016/j.jcf.2008.03.009.

[3] C. Férec, V. Scotet, Genetics of cystic fibrosis: Basics, Archives de Pédiatrie. 27 (2020) eS4–eS7. https://doi.org/10.1016/S0929-693X(20)30043-9.

[4] B. Kerem, J.M. Rommens, J.A. Buchanan, D. Markiewicz, T.K. Cox, A. Chakravarti, M. Buchwald, L.C. Tsui, Identification of the cystic fibrosis gene: genetic analysis, Science. 245 (1989) 1073–1080. https://doi.org/10.1126/science.2570460.

[5] CFTR2 Variant List History | CFTR2, (n.d.). https://cftr2.org/mutations_history (accessed July 29, 2022).

[6] J.S. Elborn, Cystic fibrosis, The Lancet. 388 (2016) 2519–2531. https://doi.org/10.1016/S0140-6736(16)00576-6.

[7] J.L. Bobadilla, M. Macek, J.P. Fine, P.M. Farrell, Cystic fibrosis: A worldwide analysis of CFTR mutations—correlation with incidence data and application to screening, Human Mutation. 19 (2002) 575–606. https://doi.org/10.1002/humu.10041.

[8] N. Kamal, P. Surana, C. Koh, Liver disease in patients with cystic fibrosis, Curr Opin Gastroenterol. 34 (2018) 146–151. https://doi.org/10.1097/MOG.0000000000000432.

[9] J.R. Govan, V. Deretic, Microbial pathogenesis in cystic fibrosis: mucoid Pseudomonas aeruginosa and Burkholderia cepacia, Microbiol Rev. 60 (1996) 539–574. https://doi.org/10.1128/mr.60.3.539-574.1996.

[10] D.C. Gadsby, P. Vergani, L. Csanády, The ABC protein turned chloride channel whose failure causes cystic fibrosis, Nature. 440 (2006) 477–483. https://doi.org/10.1038/nature04712.

[11] F.L. Theodoulou, I.D. Kerr, ABC transporter research: going strong 40 years on, Biochem Soc Trans. 43 (2015) 1033–1040. https://doi.org/10.1042/BST20150139.

[12] K.P. Locher, Mechanistic diversity in ATP-binding cassette (ABC) transporters, Nat Struct Mol Biol. 23 (2016) 487–493. https://doi.org/10.1038/nsmb.3216.

[13] L. Csanády, P. Vergani, D.C. Gadsby, STRUCTURE, GATING, AND REGULATION OF THE CFTR ANION CHANNEL, Physiol Rev. 99 (2019) 707–738. https://doi.org/10.1152/physrev.00007.2018.

[14] Z. Zhang, F. Liu, J. Chen, Conformational Changes of CFTR upon Phosphorylation and ATP Binding, Cell. 170 (2017) 483-491.e8. https://doi.org/10.1016/j.cell.2017.06.041.

[15] F. Liu, Z. Zhang, L. Csanády, D.C. Gadsby, J. Chen, Molecular Structure of the Human CFTR Ion Channel, Cell. 169 (2017) 85-95.e8. https://doi.org/10.1016/j.cell.2017.02.024.

[16] N. Odolczyk, P. Zielenkiewicz, Molecular modelling approaches for cystic fibrosis transmembrane conductance regulator studies, The International Journal of Biochemistry & Cell Biology. 52 (2014) 39–46. https://doi.org/10.1016/j.biocel.2014.04.004.

[17] D.N. Sheppard, M.J. Welsh, Structure and Function of the CFTR Chloride Channel, Physiological Reviews. 79 (1999) S23–S45. https://doi.org/10.1152/physrev.1999.79.1.S23.

[18] M.P. Anderson, D.P. Rich, R.J. Gregory, A.E. Smith, M.J. Welsh, Generation of cAMP-activated chloride currents by expression of CFTR, Science. 251 (1991) 679–682. https://doi.org/10.1126/science.1704151.

[19] Y. Wang, J.A. Wrennall, Z. Cai, H. Li, D.N. Sheppard, Understanding how cystic fibrosis mutations disrupt CFTR function: From single molecules to animal models, The International Journal of Biochemistry & Cell Biology. 52 (2014) 47–57. https://doi.org/10.1016/j.biocel.2014.04.001.

[20] F. Becq, M.A. Mall, D.N. Sheppard, M. Conese, O. Zegarra-Moran, Pharmacological therapy for cystic fibrosis: From bench to bedside, Journal of Cystic Fibrosis. 10 (2011) S129–S145. https://doi.org/10.1016/S1569-1993(11)60018-0.

[21] S.M. Rowe, A.S. Verkman, Cystic Fibrosis Transmembrane Regulator Correctors and Potentiators, Cold Spring Harb Perspect Med. 3 (2013) a009761. https://doi.org/10.1101/cshperspect.a009761.

[22] K.-Y. Jih, W.-Y. Lin, Y. Sohma, T.-C. Hwang, CFTR potentiators: from bench to bedside, Current Opinion in Pharmacology. 34 (2017) 98–104. https://doi.org/10.1016/j.coph.2017.09.015.

[23] F. Van Goor, H. Yu, B. Burton, B.J. Hoffman, Effect of ivacaftor on CFTR forms with missense mutations associated with defects in protein processing or function, J Cyst Fibros. 13 (2014) 29–36. https://doi.org/10.1016/j.jcf.2013.06.008.

[24] B.W. Ramsey, J. Davies, N.G. McElvaney, E. Tullis, S.C. Bell, P. Dřevínek, M. Griese, E.F. McKone, C.E. Wainwright, M.W. Konstan, R. Moss, F. Ratjen, I. Sermet-Gaudelus, S.M. Rowe, Q. Dong, S. Rodriguez, K. Yen, C. Ordoñez, J.S. Elborn, A CFTR Potentiator in Patients with Cystic Fibrosis and the G551D Mutation, Http://Dx.Doi.Org/10.1056/NEJMoa1105185. (2011). https://doi.org/10.1056/NEJMoa1105185.

[25] T.W. Loo, M.C. Bartlett, D.M. Clarke, Correctors promote folding of the CFTR in the endoplasmic reticulum, Biochem J. 413 (2008) 29–36. https://doi.org/10.1042/BJ20071690.

[26] S.M. Rowe, S.A. McColley, E. Rietschel, X. Li, S.C. Bell, M.W. Konstan, G. Marigowda, D. Waltz, M.P. Boyle, VX09-809-102 Study Group, Lumacaftor/Ivacaftor Treatment of Patients with Cystic Fibrosis Heterozygous for F508del-CFTR, Ann Am Thorac Soc. 14 (2017) 213–219. https://doi.org/10.1513/AnnalsATS.201609-689OC.

[27] J.L. Taylor-Cousar, M. Jain, T.L. Barto, T. Haddad, J. Atkinson, S. Tian, R. Tang, G. Marigowda, D. Waltz, J. Pilewski, VX14-809-106 Investigator Group, Lumacaftor/ivacaftor in patients with cystic fibrosis and advanced lung disease homozygous for F508del-CFTR, J Cyst Fibros. 17 (2018) 228–235. https://doi.org/10.1016/j.jcf.2017.09.012.

[28] S.M. Rowe, C. Daines, F.C. Ringshausen, E. Kerem, J. Wilson, E. Tullis, N. Nair, C. Simard, L. Han, E.P. Ingenito, C. McKee, J. Lekstrom-Himes, J.C. Davies, Tezacaftor-Ivacaftor in Residual-Function Heterozygotes with Cystic Fibrosis, N Engl J Med. 377 (2017) 2024–2035. https://doi.org/10.1056/NEJMoa1709847.

[29] J.L. Taylor-Cousar, A. Munck, E.F. McKone, C.K. van der Ent, A. Moeller, C. Simard, L.T. Wang, E.P. Ingenito, C. McKee, Y. Lu, J. Lekstrom-Himes, J.S. Elborn, Tezacaftor-Ivacaftor in Patients with Cystic Fibrosis Homozygous for Phe508del, N Engl J Med. 377 (2017) 2013–2023. https://doi.org/10.1056/NEJMoa1709846.

[30] P.G. Middleton, M.A. Mall, P. Dřevínek, L.C. Lands, E.F. McKone, D. Polineni, B.W. Ramsey, J.L. Taylor-Cousar, E. Tullis, F. Vermeulen, G. Marigowda, C.M. McKee, S.M. Moskowitz, N. Nair, J. Savage, C. Simard, S. Tian, D. Waltz, F. Xuan, S.M. Rowe, R. Jain, VX17-445-102 Study Group, Elexacaftor-Tezacaftor-Ivacaftor for Cystic Fibrosis with a Single Phe508del Allele, N Engl J Med. 381 (2019) 1809–1819. https://doi.org/10.1056/NEJMoa1908639.

[31] N. Brindani, A. Gianotti, S. Giovani, F. Giacomina, P. Di Fruscia, F. Sorana, S.M. Bertozzi, G. Ottonello, L. Goldoni, I. Penna, D. Russo, M. Summa, R. Bertorelli, L. Ferrera, E. Pesce, E. Sondo, L.J.V. Galietta, T. Bandiera, N. Pedemonte, F. Bertozzi, Identification, Structure-Activity Relationship, and Biological Characterization of 2,3,4,5-Tetrahydro-1H-pyrido[4,3-b]indoles as a Novel Class of CFTR Potentiators, J Med Chem. 63 (2020) 11169–11194. https://doi.org/10.1021/acs.jmedchem.0c01050.

[32] L. Froux, A. Elbahnsi, B. Boucherle, A. Billet, N. Baatallah, B. Hoffmann, J. Alliot, R. Zelli, W. Zeinyeh, R. Haudecoeur, B. Chevalier, A. Fortuné, S. Mirval, C. Simard, P. Lehn, J.-P. Mornon, A. Hinzpeter, F. Becq, I. Callebaut, J.-L. Décout, Targeting different binding sites in the CFTR structures allows to synergistically potentiate channel activity, Eur J Med Chem. 190 (2020) 112116. https://doi.org/10.1016/j.ejmech.2020.112116.

[33] P.-W. Phuan, J.-A. Tan, A.A. Rivera, L. Zlock, D.W. Nielson, W.E. Finkbeiner, P.M. Haggie, A.S. Verkman, Nanomolar-potency “co-potentiator” therapy for cystic fibrosis caused by a defined subset of minimal function CFTR mutants, Sci Rep. 9 (2019) 17640. https://doi.org/10.1038/s41598-019-54158-2.

[34] N. Pedemonte, F. Bertozzi, E. Caci, F. Sorana, P. Di Fruscia, V. Tomati, L. Ferrera, A. Rodríguez-Gimeno, F. Berti, E. Pesce, E. Sondo, A. Gianotti, P. Scudieri, T. Bandiera, L.J.V. Galietta, Discovery of a picomolar potency pharmacological corrector of the mutant CFTR chloride channel, Sci Adv. 6 (2020) eaay9669. https://doi.org/10.1126/sciadv.aay9669.

[35] G. Faure, H. Xu, F.A. Saul, Crystal Structure of Crotoxin Reveals Key Residues Involved in the Stability and Toxicity of This Potent Heterodimeric β-Neurotoxin, Journal of Molecular Biology. 412 (2011) 176–191. https://doi.org/10.1016/j.jmb.2011.07.027.

[36] G. Faure, N. Bakouh, S. Lourdel, N. Odolczyk, A. Premchandar, N. Servel, A. Hatton, M.K. Ostrowski, H. Xu, F.A. Saul, C. Moquereau, S. Bitam, I. Pranke, G. Planelles, J. Teulon, H. Herrmann, A. Roldan, P. Zielenkiewicz, M. Dadlez, G.L. Lukacs, I. Sermet-Gaudelus, M. Ollero, P.-J. Corringer, A. Edelman, Rattlesnake Phospholipase A2 Increases CFTR-Chloride Channel Current and Corrects Δ F508CFTR Dysfunction: Impact in Cystic Fibrosis, Journal of Molecular Biology. 428 (2016) 2898–2915. https://doi.org/10.1016/j.jmb.2016.05.016.

[37] D. Nemecz, M. Ostrowski, M. Ravatin, F. Saul, G. Faure, Crystal Structure of Isoform CBd of the Basic Phospholipase A2 Subunit of Crotoxin: Description of the Structural Framework of CB for Interaction with Protein Targets, Molecules. 25 (2020) E5290. https://doi.org/10.3390/molecules25225290.

[38] G. Faure, D. Porowinska, F. Saul, Crotoxin from Crotalus durissus terrificus and Crotoxin-Related Proteins: Structure and Function Relationship, in: L.J. Cruz, S. Luo, P. Gopalakrishnakone (Eds.), Toxins and Drug Discovery, Springer Netherlands, Dordrecht, 2017: pp. 3–20. https://doi.org/10.1007/978-94-007-6452-1_7.

[39] A. Vangone, R. Spinelli, V. Scarano, L. Cavallo, R. Oliva, COCOMAPS: a web application to analyze and visualize contacts at the interface of biomolecular complexes, Bioinformatics. 27 (2011) 2915–2916. https://doi.org/10.1093/bioinformatics/btr484.

[40] S.J. de Vries, M. van Dijk, A.M.J.J. Bonvin, The HADDOCK web server for data-driven biomolecular docking, Nat Protoc. 5 (2010) 883–897. https://doi.org/10.1038/nprot.2010.32.

[41] G.C.P. van Zundert, J.P.G.L.M. Rodrigues, M. Trellet, C. Schmitz, P.L. Kastritis, E. Karaca, A.S.J. Melquiond, M. van Dijk, S.J. de Vries, A.M.J.J. Bonvin, The HADDOCK2.2 Web Server:

User-Friendly Integrative Modeling of Biomolecular Complexes, Journal of Molecular Biology. 428 (2016) 720–725. https://doi.org/10.1016/j.jmb.2015.09.014.

[42] F. Van Goor, S. Hadida, P.D.J. Grootenhuis, B. Burton, D. Cao, T. Neuberger, A. Turnbull, A. Singh, J. Joubran, A. Hazlewood, J. Zhou, J. McCartney, V. Arumugam, C. Decker, J. Yang, C. Young, E.R. Olson, J.J. Wine, R.A. Frizzell, M. Ashlock, P. Negulescu, Rescue of CF airway epithelial cell function in vitro by a CFTR potentiator, VX-770, Proc Natl Acad Sci U S A. 106 (2009) 18825–18830. https://doi.org/10.1073/pnas.0904709106.

[43] F. Van Goor, S. Hadida, P.D.J. Grootenhuis, B. Burton, J.H. Stack, K.S. Straley, C.J. Decker, M. Miller, J. McCartney, E.R. Olson, J.J. Wine, R.A. Frizzell, M. Ashlock, P.A. Negulescu, Correction of the F508del-CFTR protein processing defect in vitro by the investigational drug VX-809, Proc Natl Acad Sci U S A. 108 (2011) 18843–18848. https://doi.org/10.1073/pnas.1105787108.

[44] D. Keating, G. Marigowda, L. Burr, C. Daines, M.A. Mall, E.F. McKone, B.W. Ramsey, S.M. Rowe, L.A. Sass, E. Tullis, C.M. McKee, S.M. Moskowitz, S. Robertson, J. Savage, C. Simard, F. Van Goor, D. Waltz, F. Xuan, T. Young, J.L. Taylor-Cousar, VX-445–Tezacaftor–Ivacaftor in Patients with Cystic Fibrosis and One or Two Phe508del Alleles, N Engl J Med. 379 (2018) 1612–1620. https://doi.org/10.1056/NEJMoa1807120.

[45] H.Y. Ren, D.E. Grove, O. De La Rosa, S.A. Houck, P. Sopha, F. Van Goor, B.J. Hoffman, D.M. Cyr, VX-809 corrects folding defects in cystic fibrosis transmembrane conductance regulator protein through action on membrane-spanning domain 1, Mol Biol Cell. 24 (2013) 3016–3024. https://doi.org/10.1091/mbc.E13-05-0240.

[46] R.P. Hudson, J.E. Dawson, P.A. Chong, Z. Yang, L. Millen, P.J. Thomas, C.G. Brouillette, J.D. Forman-Kay, Direct Binding of the Corrector VX-809 to Human CFTR NBD1: Evidence of an Allosteric Coupling between the Binding Site and the NBD1:CL4 Interface, Mol Pharmacol. 92 (2017) 124–135. https://doi.org/10.1124/mol.117.108373.

[47] G. Veit, A. Roldan, M.A. Hancock, D.F. Da Fonte, H. Xu, M. Hussein, S. Frenkiel, E. Matouk, T. Velkov, G.L. Lukacs, Allosteric folding correction of F508del and rare CFTR mutants by

elexacaftor-tezacaftor-ivacaftor (Trikafta) combination, JCI Insight. 5 (2020) 139983. https://doi.org/10.1172/jci.insight.139983.

[48] N. Baatallah, A. Elbahnsi, J.-P. Mornon, B. Chevalier, I. Pranke, N. Servel, R. Zelli, J.-L. Décout, A. Edelman, I. Sermet-Gaudelus, I. Callebaut, A. Hinzpeter, Pharmacological chaperones improve intra-domain stability and inter-domain assembly via distinct binding sites to rescue misfolded CFTR, Cell Mol Life Sci. 78 (2021) 7813–7829. https://doi.org/10.1007/s00018-021-03994-5.

[49] K. Fiedorczuk, J. Chen, Mechanism of CFTR correction by type I folding correctors, Cell. 185 (2022) 158-168.e11. https://doi.org/10.1016/j.cell.2021.12.009.

[50] F. Liu, Z. Zhang, A. Levit, J. Levring, K.K. Touhara, B.K. Shoichet, J. Chen, Structural identification of a hotspot on CFTR for potentiation, Science. 364 (2019) 1184–1188. https://doi.org/10.1126/science.aaw7611.

[51] V. Sala, S.J. Cnudde, A. Murabito, A. Massarotti, E. Hirsch, A. Ghigo, Therapeutic peptides for the treatment of cystic fibrosis: Challenges and perspectives, European Journal of Medicinal Chemistry. 213 (2021) 113191. https://doi.org/10.1016/j.ejmech.2021.113191.

[52] L. Ferrera, F. Cappiello, M.R. Loffredo, E. Puglisi, B. Casciaro, B. Botta, L.J.V. Galietta, M. Mori, M.L. Mangoni, Esc peptides as novel potentiators of defective cystic fibrosis transmembrane conductance regulator: an unprecedented property of antimicrobial peptides, Cell Mol Life Sci. 79 (2021) 67. https://doi.org/10.1007/s00018-021-04030-2.

[53] S.G. Bompadre, M. Li, T.-C. Hwang, Mechanism of G551D-CFTR (cystic fibrosis transmembrane conductance regulator) potentiation by a high affinity ATP analog, J Biol Chem. 283 (2008) 5364–5369. https://doi.org/10.1074/jbc.M709417200.

[54] M.-F. Tsai, K.-Y. Jih, H. Shimizu, M. Li, T.-C. Hwang, Optimization of the degenerated interfacial ATP binding site improves the function of disease-related mutant cystic fibrosis transmembrane conductance regulator (CFTR) channels, J Biol Chem. 285 (2010) 37663–37671. https://doi.org/10.1074/jbc.M110.172817.

[55] Z. Zhou, X. Wang, M. Li, Y. Sohma, X. Zou, T.-C. Hwang, High affinity ATP/ADP analogues as new tools for studying CFTR gating, J Physiol. 569 (2005) 447–457. https://doi.org/10.1113/jphysiol.2005.095083.

[56] A.A. Aleksandrov, L. Aleksandrov, J.R. Riordan, Nucleoside triphosphate pentose ring impact on CFTR gating and hydrolysis, FEBS Lett. 518 (2002) 183–188. https://doi.org/10.1016/s0014-5793(02)02698-4.

[57] Z. Cai, A. Taddei, D.N. Sheppard, Differential sensitivity of the cystic fibrosis (CF)-associated mutants G551D and G1349D to potentiators of the cystic fibrosis transmembrane conductance regulator (CFTR) Cl- channel, J Biol Chem. 281 (2006) 1970–1977. https://doi.org/10.1074/jbc.M510576200.

[58] H. Miki, Z. Zhou, M. Li, T.-C. Hwang, S.G. Bompadre, Potentiation of disease-associated cystic fibrosis transmembrane conductance regulator mutants by hydrolyzable ATP analogs, J Biol Chem. 285 (2010) 19967–19975. https://doi.org/10.1074/jbc.M109.092684.

[59] K.-Y. Jih, W.-Y. Lin, Y. Sohma, T.-C. Hwang, CFTR potentiators: from bench to bedside, Curr Opin Pharmacol. 34 (2017) 98–104. https://doi.org/10.1016/j.coph.2017.09.015.

[60] F. Weinreich, P.G. Wood, J.R. Riordan, G. Nagel, Direct action of genistein on CFTR, Pflugers Arch. 434 (1997) 484–491. https://doi.org/10.1007/s004240050424.

[61] A. Schmidt, L.K. Hughes, Z. Cai, F. Mendes, H. Li, D.N. Sheppard, M.D. Amaral, Prolonged treatment of cells with genistein modulates the expression and function of the cystic fibrosis transmembrane conductance regulator, Br J Pharmacol. 153 (2008) 1311–1323. https://doi.org/10.1038/sj.bjp.0707663.

[62] O. Moran, L.J.V. Galietta, O. Zegarra-Moran, Binding site of activators of the cystic fibrosis transmembrane conductance regulator in the nucleotide binding domains, Cell Mol Life Sci. 62 (2005) 446–460. https://doi.org/10.1007/s00018-004-4422-3.

[63] L. Froux, A. Elbahnsi, B. Boucherle, A. Billet, N. Baatallah, B. Hoffmann, J. Alliot, R. Zelli, W. Zeinyeh, R. Haudecoeur, B. Chevalier, A. Fortuné, S. Mirval, C. Simard, P. Lehn, J.-P. Mornon, A. Hinzpeter, F. Becq, I. Callebaut, J.-L. Décout, Targeting different binding sites in the CFTR

structures allows to synergistically potentiate channel activity, Eur J Med Chem. 190 (2020) 112116. https://doi.org/10.1016/j.ejmech.2020.112116.

[64] G. Veit, D.F. Da Fonte, R.G. Avramescu, A. Premchandar, M. Bagdany, H. Xu, D. Bensinger, D. Stubba, B. Schmidt, E. Matouk, G.L. Lukacs, Mutation-specific dual potentiators maximize rescue of CFTR gating mutants, J Cyst Fibros. 19 (2020) 236–244. https://doi.org/10.1016/j.jcf.2019.10.011.

[65] A. Billet, Y. Jia, T.J. Jensen, Y.-X. Hou, X.-B. Chang, J.R. Riordan, J.W. Hanrahan, Potential sites of CFTR activation by tyrosine kinases, Channels (Austin). 10 (2016) 247–251. https://doi.org/10.1080/19336950.2015.1126010.

[66] Y. Kim, I. Jun, D.H. Shin, J.G. Yoon, H. Piao, J. Jung, H.W. Park, M.H. Cheng, I. Bahar, D.C. Whitcomb, M.G. Lee, Regulation of CFTR Bicarbonate Channel Activity by WNK1: Implications for Pancreatitis and CFTR-Related Disorders, Cell Mol Gastroenterol Hepatol. 9 (2020) 79–103. https://doi.org/10.1016/j.jcmgh.2019.09.003.

[67] W.M. Rabeh, F. Bossard, H. Xu, T. Okiyoneda, M. Bagdany, C.M. Mulvihill, K. Du, S. di Bernardo, Y. Liu, L. Konermann, A. Roldan, G.L. Lukacs, Correction of both NBD1 energetics and domain interface is required to restore ΔF508 CFTR folding and function, Cell. 148 (2012) 150–163. https://doi.org/10.1016/j.cell.2011.11.024.

[68] H.M. Berman, J. Westbrook, Z. Feng, G. Gilliland, T.N. Bhat, H. Weissig, I.N. Shindyalov, P.E. Bourne, The Protein Data Bank, Nucleic Acids Res. 28 (2000) 235–242. https://doi.org/10.1093/nar/28.1.235.

[69] E. de Castro, C.J.A. Sigrist, A. Gattiker, V. Bulliard, P.S. Langendijk-Genevaux, E. Gasteiger, A. Bairoch, N. Hulo, ScanProsite: detection of PROSITE signature matches and ProRule-associated functional and structural residues in proteins, Nucleic Acids Res. 34 (2006) W362–W365. https://doi.org/10.1093/nar/gkl124.

[70] E. Deplazes, J. Davies, A.M.J.J. Bonvin, G.F. King, A.E. Mark, Combination of Ambiguous and Unambiguous Data in the Restraint-driven Docking of Flexible Peptides with HADDOCK: The Binding of the Spider Toxin PcTx1 to the Acid Sensing Ion Channel (ASIC) 1a, J. Chem. Inf. Model. 56 (2016) 127–138. https://doi.org/10.1021/acs.jcim.5b00529.

[71] C. Geng, S. Narasimhan, J.P.G.L.M. Rodrigues, A.M.J.J. Bonvin, Information-Driven, Ensemble Flexible Peptide Docking Using HADDOCK, in: O. Schueler-Furman, N. London (Eds.), Modeling Peptide-Protein Interactions: Methods and Protocols, Springer New York, New York, NY, 2017: pp. 109–138. https://doi.org/10.1007/978-1-4939-6798-8_8.

[72] P. Fanen, R. Labarthe, F. Garnier, M. Benharouga, M. Goossens, A. Edelman, Cystic fibrosis phenotype associated with pancreatic insufficiency does not always reflect the cAMP-dependent chloride conductive pathway defect. Analysis of C225R-CFTR and R1066C-CFTR, J Biol Chem. 272 (1997) 30563–30566. https://doi.org/10.1074/jbc.272.48.30563.

[73] N. Odolczyk, J. Fritsch, C. Norez, N. Servel, M.F. da Cunha, S. Bitam, A. Kupniewska, L. Wiszniewski, J. Colas, K. Tarnowski, D. Tondelier, A. Roldan, E.L. Saussereau, P. Melin-Heschel, G. Wieczorek, G.L. Lukacs, M. Dadlez, G. Faure, H. Herrmann, M. Ollero, F. Becq, P. Zielenkiewicz, A. Edelman, Discovery of novel potent ΔF508-CFTR correctors that target the nucleotide binding domain, EMBO Mol Med. 5 (2013) 1484–1501. https://doi.org/10.1002/emmm.201302699.

[74] J. Mutterer, E. Zinck, Quick-and-clean article figures with FigureJ, J Microsc. 252 (2013) 89–91. https://doi.org/10.1111/jmi.12069.

[75] A.E. Derome, M.P. Williamson, Rapid-pulsing artifacts in double-quantum-filtered COSY, Journal of Magnetic Resonance (1969). 88 (1990) 177–185. https://doi.org/10.1016/0022-2364(90)90123-Q.

[76] D.J. States, R.A. Haberkorn, D.J. Ruben, A two-dimensional nuclear overhauser experiment with pure absorption phase in four quadrants, Journal of Magnetic Resonance (1969). 48 (1982) 286–292. https://doi.org/10.1016/0022-2364(82)90279-7.

[77] M.J. Thrippleton, J. Keeler, Elimination of Zero-Quantum Interference in Two-Dimensional NMR Spectra, Angewandte Chemie International Edition. 42 (2003) 3938–3941. https://doi.org/10.1002/anie.200351947.

[78] A. Bax, D.G. Davis, Practical aspects of two-dimensional transverse NOE spectroscopy, Journal of Magnetic Resonance (1969). 63 (1985) 207–213. https://doi.org/10.1016/0022-2364(85)90171-4.

[79] M. Mayer, B. Meyer, Group Epitope Mapping by Saturation Transfer Difference NMR To Identify Segments of a Ligand in Direct Contact with a Protein Receptor, J. Am. Chem. Soc. 123 (2001) 6108–6117. https://doi.org/10.1021/ja0100120.

[80] H. Geen, R. Freeman, Band-selective radiofrequency pulses, Journal of Magnetic Resonance (1969). 93 (1991) 93–141. https://doi.org/10.1016/0022-2364(91)90034-Q.

## Tables

### Table 1. Automated patch-clamp (QPatch) results for active peptides of Series I, II and III.

| | Peptide | Sequences | Controls in presence of activation cocktail [Mean ± SEM] (n) | Peptide concentration [µM] | Experimental values in presence of activation cocktail + peptide [Mean ± SEM] (n) | p-values of comparisons vs associated controls | Experimental values summarized in presence of activation cocktail + Vx770 [Mean ± SEM] (n) | Experimental values summarized in presence of activation cocktail + VX-770 + peptide [Mean ± SEM] (n) | p-values of comparisons vs associated controls |
|---|---|---|---|---|---|---|---|---|---|
| Series I | A | 1-HLLQFNKMIKFETRKN-16 | 55 ± 47 (n = 4) | 5 | 46 ± 19 (n = 4) | 0.231 | 71 ± 50 (n = 4) | 92 ± 24 (n = 4) | 0.885 |
| | | | | 50 | 82 ± 38 (n = 4) | 0.238 | | 154 ± 35 (n = 4) | 0.021 |
| | A2 | 1-HLLQFNK-7 | 88 ± 22 (n = 7) | 5 | 76 ± 21 (n = 7) | 0.417 | 127 ± 16 (n = 7) | 102 ± 31 (n = 7) | 0.108 |
| | | | | 50 | 131 ± 36 (n = 10) | 0.011 | | 173 ± 54 (n = 10) | 0.157 |
| | B | 16-NAVPFYAFYGCYCGWGGQ-33 | 77 ± 23 (n = 6) | 5 | 91 ± 24 (n = 6) | 0.552 | 143 ± 23 (n = 6) | 181 ± 42 (n = 6) | 0.233 |
| | | | | 50 | 161 ± 47 (n = 5) | <0.0001 | | 194 ± 64 (n = 5) | 0.234 |
| | C | 105-NGYMFYPDS-113 | 45 ± 18 (n = 7) | 5 | 77 ± 18 (n = 4) | 0.046 | 93 ± 15 (n = 7) | 105 ± 11 (n = 4) | 0.636 |
| | | | | 50 | 76 ± 28 (n = 9) | 0.013 | | 125 ± 24 (n = 9) | 0.013 |
| | C1 | 107-YMFYPDSR-114 | 38 ± 14 (n = 6) | 5 | 53 ± 17 (n = 6) | 0.161 | 121 ± 37 (n = 6) | 182 ± 33 (n = 6) | 0.024 |
| | | | | 50 | 30 ±10 (n = 7) | 0.240 | | 101 ± 21 (n = 7) | 0.183 |
| | C2 | 108-MFYPDSR-114 | 28 ± 17 (n = 8) | 5 | 53 ± 10 (n = 8) | 0.031 | 98 ± 33 (n = 8) | 124 ± 33 (n = 8) | 0.141 |
| | | | | 50 | 60 ± 14 (n = 7) | 0.005 | | 139 ± 27 (n = 7) | 0.019 |
| Series II | N3 | 16-NAVPFSAFSGCDSGWGGQ-33 I 108-MFYPDSRC-115 | 72 ± 10 (n = 6) | 5 | 118 ± 41 (n = 4) | 0.018 | 96 ± 11 (n = 6) | 150 ± 57 (n = 4) | 0.0085 |
| | | | | 50 | 105 ± 8 (n = 7) | 0.0007 | | 149 ± 25 (n = 7) | 0.0001 |
| Series III | M2 | FVDQFKAEW | 52 ± 9 (n = 5) | 5 | 118 ± 49 (n = 4) | 0.0018 | 94 ± 20 (n = 5) | 100 ± 33 (n = 4) | 0.0185 |
| | | | | 50 | 184 ± 74 (n = 7) | 0.0030 | | 153 ± 48 (n = 7) | 0.0185 |
| | M3 | FRKNFSKDW | 37 ± 27 (n = 5) | 5 | 65 ± 14 (n = 5) | 0.0228 | 65 ± 32 (n = 5) | 114 ± 27 (n = 5) | 0.0092 |
| | | | | 50 | 97 ± 33 (n = 6) | 0.0014 | | 150 ± 44 (n = 6) | 0.0002 |
| | M10 | FRKDFETFW | 38 ± 10 (n = 6) | 5 | 94 ± 24 (n = 4) | 0.0004 | 66 ± 20 (n = 6) | 174 ± 21 (n = 4) | <0.0001 |
| | | | | 50 | 69 ± 18 (n = 7) | 0.0194 | | 108 ± 24 (n = 7) | 0.0016 |

Experimental values are given as mean ± SEM; SEM - standard error of the mean; n - probes in each experiment; p-value has been calculated from statistical analysis (ANOVA test) to compare the peptide with forskolin (or with forskolin and VX-770) versus the associated control p-values are underlined when < 0.05.

## Figures

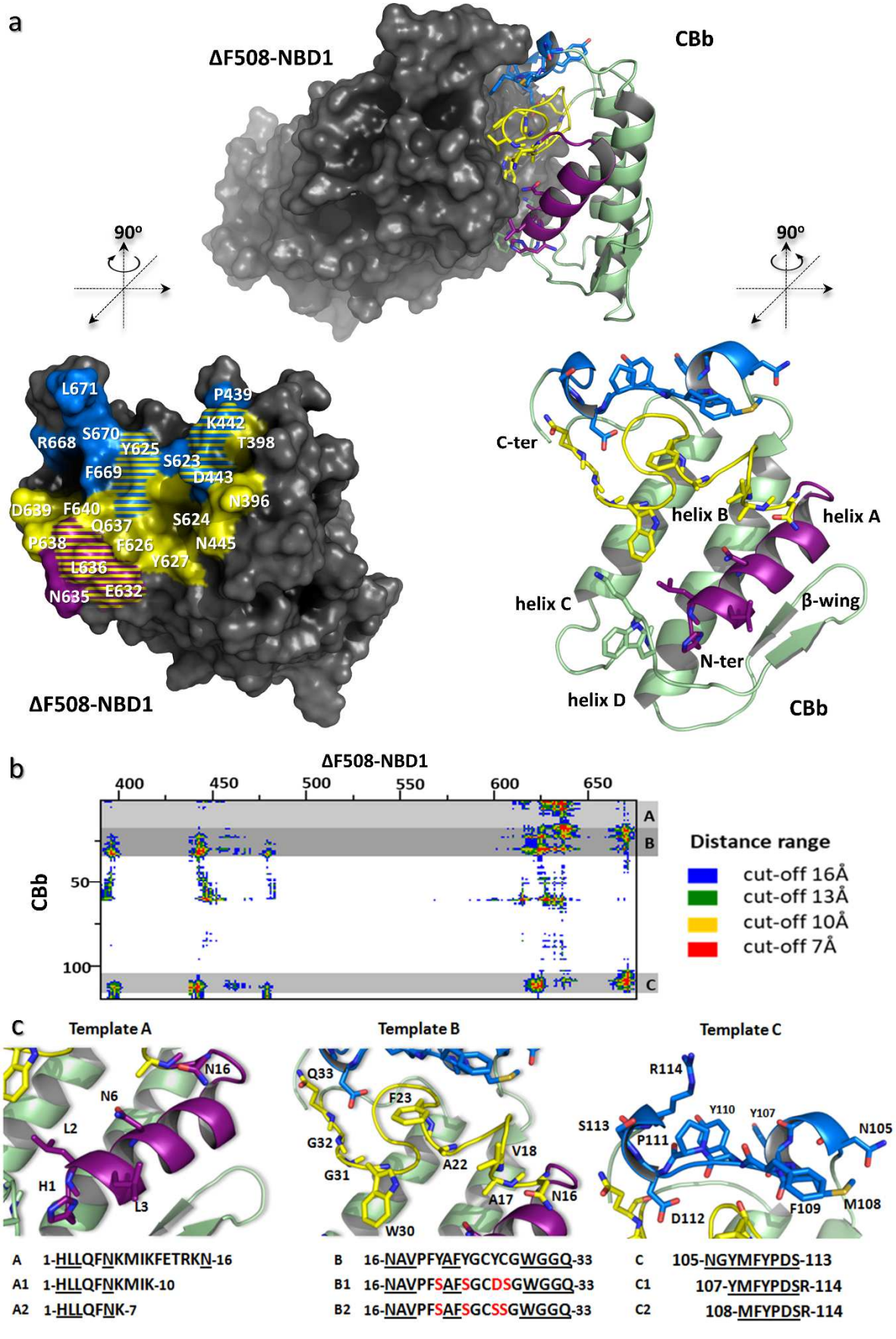
a
ΔF508-NBD1
CBb
90°
90°
L671
P439
K442
R668
S670
T398
Y625
S623
F669
D443
N396
D639
F640
Q637
S624
P638
F626
N445
Y627
L636
N635
E632
ΔF508-NBD1
C-ter
helix B
helix A
helix C
β-wing
N-ter
helix D
CBb
b
ΔF508-NBD1
400
450
500
550
600
650
CBb
50
100
A
B
C
Distance range
cut-off 16Å
cut-off 13Å
cut-off 10Å
cut-off 7Å
C
Template A
Template B
Template C
N16
N6
L2
H1
L3
Q33
F23
G32
V18
A22
G31
A17
N16
W30
R114
Y110
Y107
S113
N105
P111
D112
F109
M108
A 1-HLLQFNKMIKFETRKN-16
A1 1-HLLQFNKMIK-10
A2 1-HLLQFNK-7
B 16-NAVPFYAFYGCYCGWGGQ-33
B1 16-NAVPFSAFSGCDSGWGGQ-33
B2 16-NAVPFSAFSGCSSGWGGQ-33
C 105-NGYMFYPDS-113
C1 107-YMFYPDSR-114
C2 108-MFYPDSR-114

**Figure 1. Analysis of the CBb and ΔF508NBD1 interaction interface and CBb template-based modeling of Series I peptides.** (a) Upper panel: Model of the CBb and ΔF508NBD1 complex. NBD1 is shown as a grey solvent accessible surface area, whereas CBb is visualized as ribbons. Lower panel: The CBb fragments selected as templates A, B and C for peptides and their cognate interface on ΔF508NBD1, are depicted in magenta, yellow and blue, respectively (lower panels). The structures of ΔF508NBD1 (clockwise) and CBb (counter clockwise) are rotated by 90° relative to the orientation shown in the upper panel. (b) Distance range map of the intermolecular contacts between CBb and ΔF508NBD1 interface residues; red, yellow, green, and blue dots indicate contacts within 7, 10, 13 and 16 Å, respectively. The CBb protein regions selected for peptide templates are highlighted in grey. (c) Close up of the A, B, and C regions selected as initial templates, together with the corresponding sequences and the proposed derived peptides. The residues in close contact with ΔF508-NBD1 are shown as sticks and are underlined in the sequences. Mutations introduced to initial peptide B are highlighted in red.

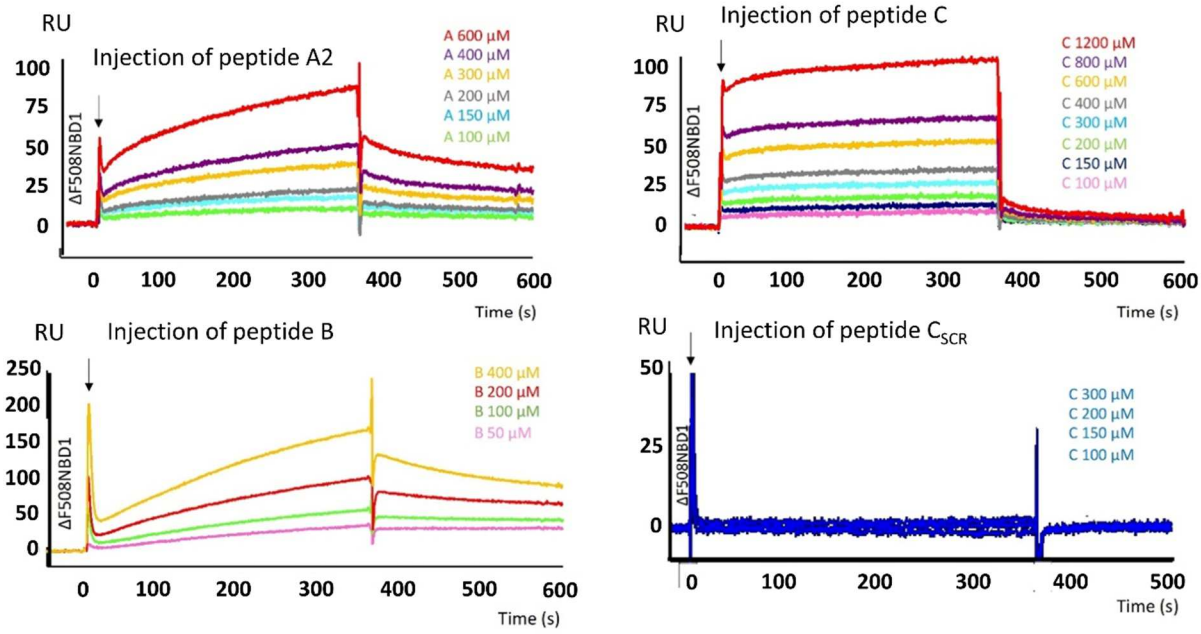


**Figure 2. SPR analysis of A2, B and C peptides binding to human CFTR ΔF508NBD1 domain.** Sensograms showing peptides binding to immobilized ΔF508NBD1. The peptide concentrations are indicated for each curve (µM). No binding of the negative control peptides $C_{scr}$/$A2_{scr}$ (lower right panel and **Figure S2**) was observed. Independent experiments were performed at least three times.

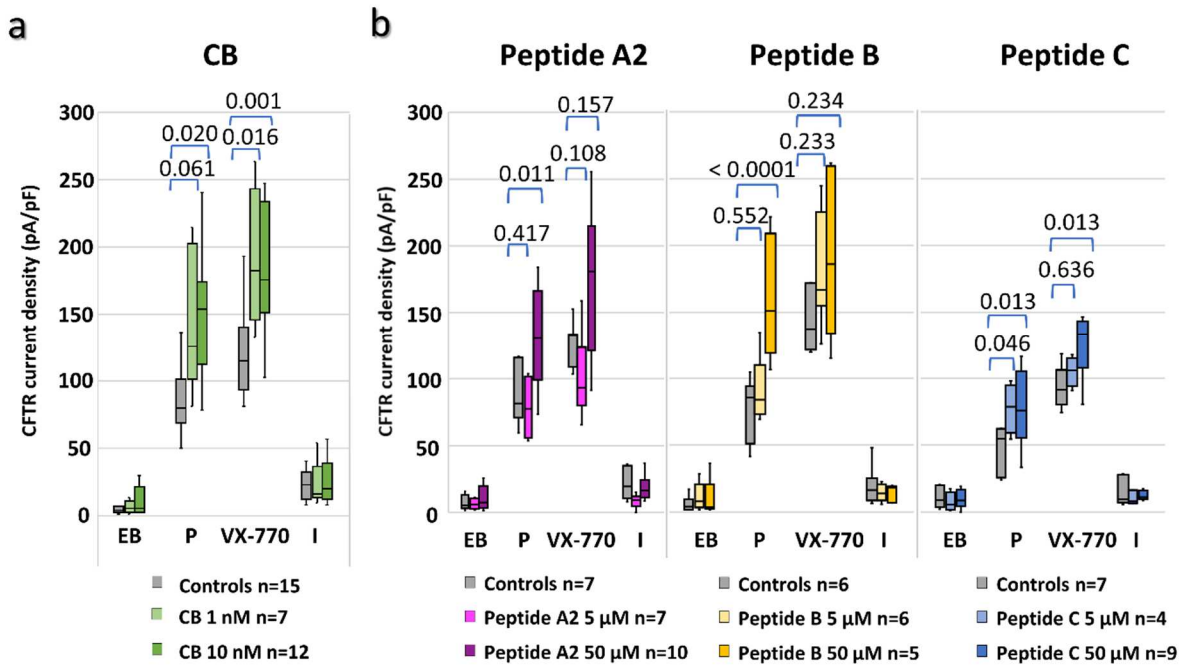


**Figure 3. Functional evaluation of CB and peptides from Series I A2, B and C by aPC technology (QPatch) in FRT cells expressing ΔF508CFTR.** Experimental values (mean, SEM) obtained after intracellular addition of (a) 1 or 10 nM CBb (b) 5 or 50 µM A2, B and C peptides. Four conditions were applied to each cell: basal (extracellular buffer; EB), phosphorylation of CFTR channel stimulated by a forskolin and IBMX cocktail (P), condition P supplemented with VX-770 and inhibition of CFTR current by Inh172 and glibenclamide compounds (I). Assays were performed on phosphorylated channels with and without VX-770. Mean current densities were calculated for each condition. Statistical analysis (Anova test) was done to compare the results without and with peptide addition (at the concentrations indicated) for each condition. P-values are shown underlined with blue horizontal brackets..

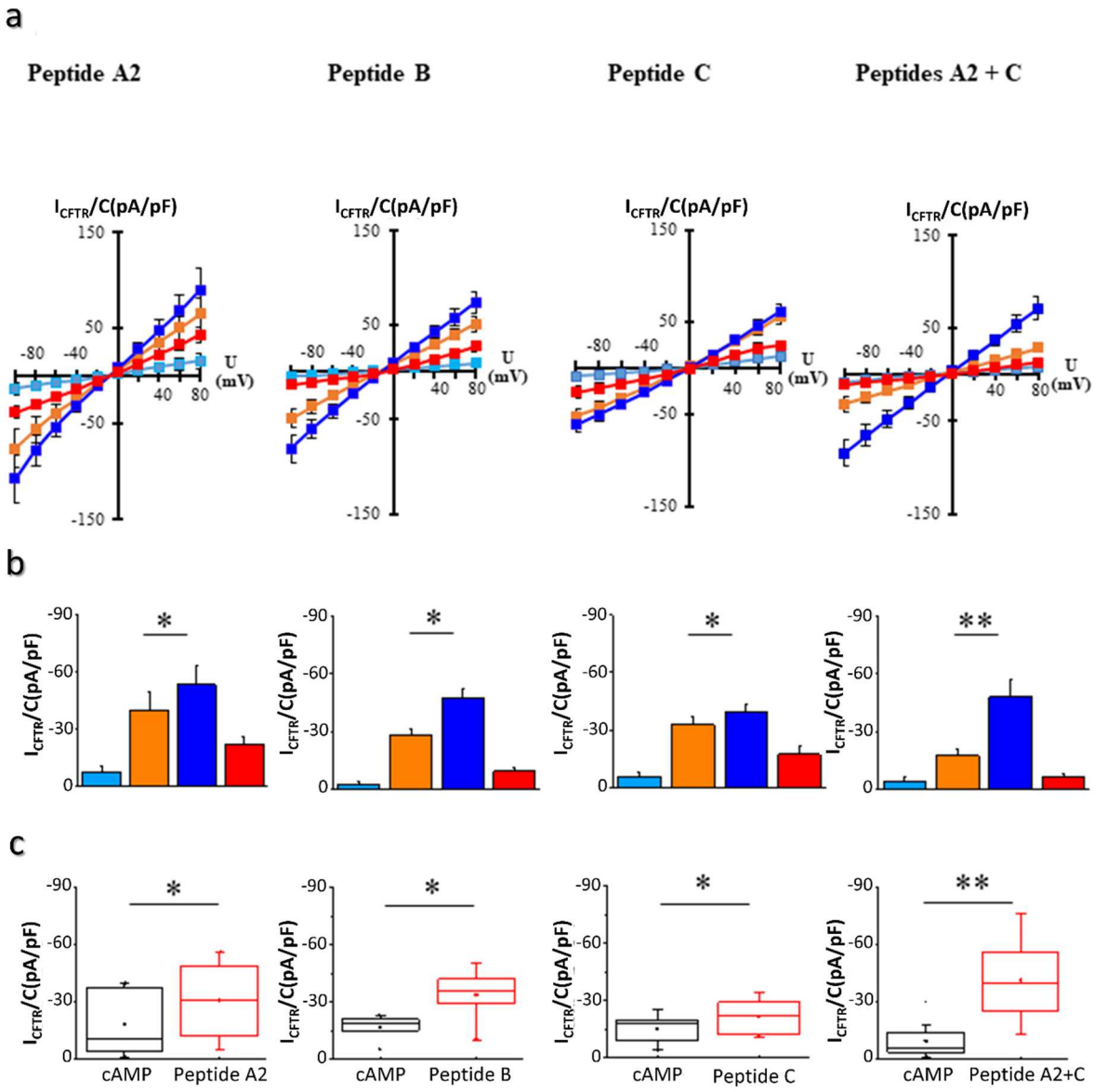


**Figure 4. Peptide activity measured by whole-cell patch-clamp recordings in HeLa or HEK293 cells expressing ΔF508CFTR.** (a) Mean (SEM) current-voltage relationships obtained in cells expressing ΔF508CFTR recorded by holding the membrane potential at 0 mV and pulsing voltages in the range from –100 mV to +80 mV at 20 mV steps: basal level (light blue), after addition of 400 µM CPT-cAMP/100 µM IBMX cocktail (orange), after addition of 1 µM peptide cocktail (dark blue) and inhibition by 5 µM $inh_{172}$/20 µM glibenclamide (red). Current densities were normalized to cell capacitance (I/C). Peptides A2

(n=7), B (n=6), C (n=5) or the (A2+C) combination (n=8, 1 µM each). (b) Histograms showing current densities at -60 mV. Cell lines were different: HEK293 ΔF508CFTR for peptide A2, HeLa ΔF508CFTR for peptides B, C and A2+C. Correction was obtained either by pharmacological chaperone (1 µM c407) for peptides C and peptides (A2+C), or by low temperature (27°C) for peptides A or B. (c) Nonparametric tests (paired sample Sign tests) were performed between cAMP and peptide cocktail responses measured at -60 mV. The four peptide cocktails significantly potentialized cAMP response at 1 µM concentration: Peptide A2 ($p=0.008$, n=7), peptide B ($p=0.016$, n=6), peptide C ($p=0.031$, n=5) and peptide (A2+C) combination ($p=0.004$, n=8). ** $p<0.005$, * $0.005<p<0.05$. Peptides A2, C and A2+C were coated with liposomes to favor internalization.

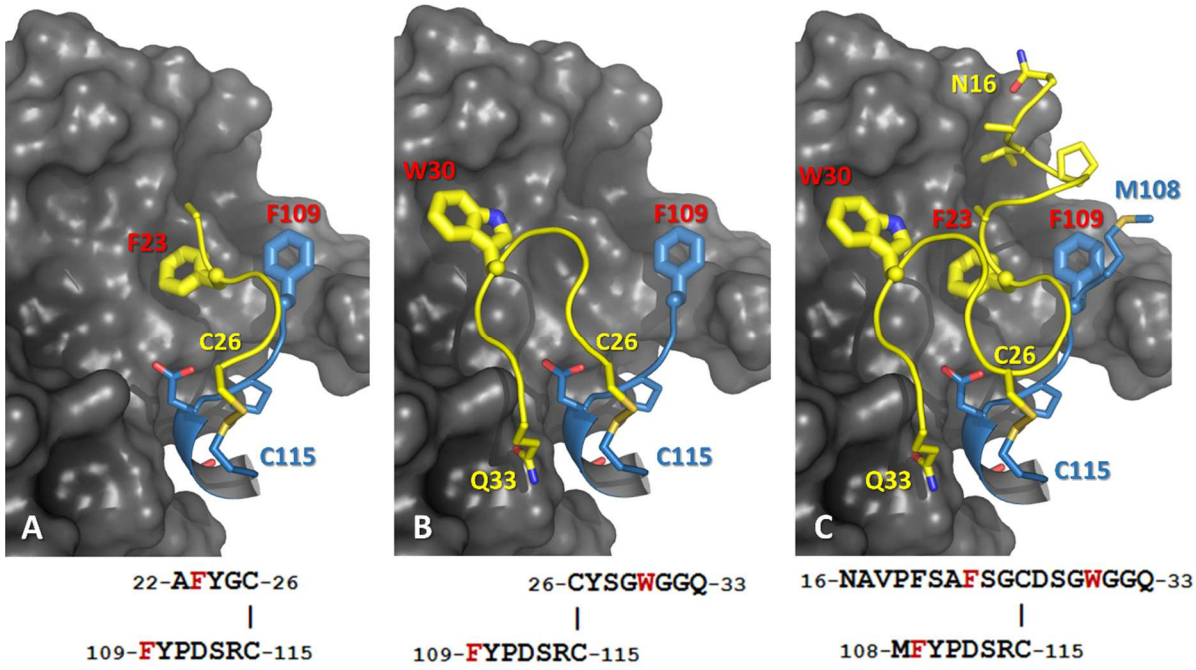


**Figure 5. Structural models of ΔF508NBD1 in complex with Series II peptides (with disulfide bond C26-C115) obtained by template based modeling.** The models of peptides (a) N1, (b) N2, and (c) N3 in complex with ΔF508NBD1 were derived from the CBb and ΔF508NBD1 complex model [36]. NBD1 is shown as a grey solvent accessible surface area, and peptides are colored according to Figure 1. CBb residues that do not contact NBD1 are not shown for clarity. Hydrophobic residues identified as crucial for the interaction with NBD1 are shown by thicker sticks and labeled in red.

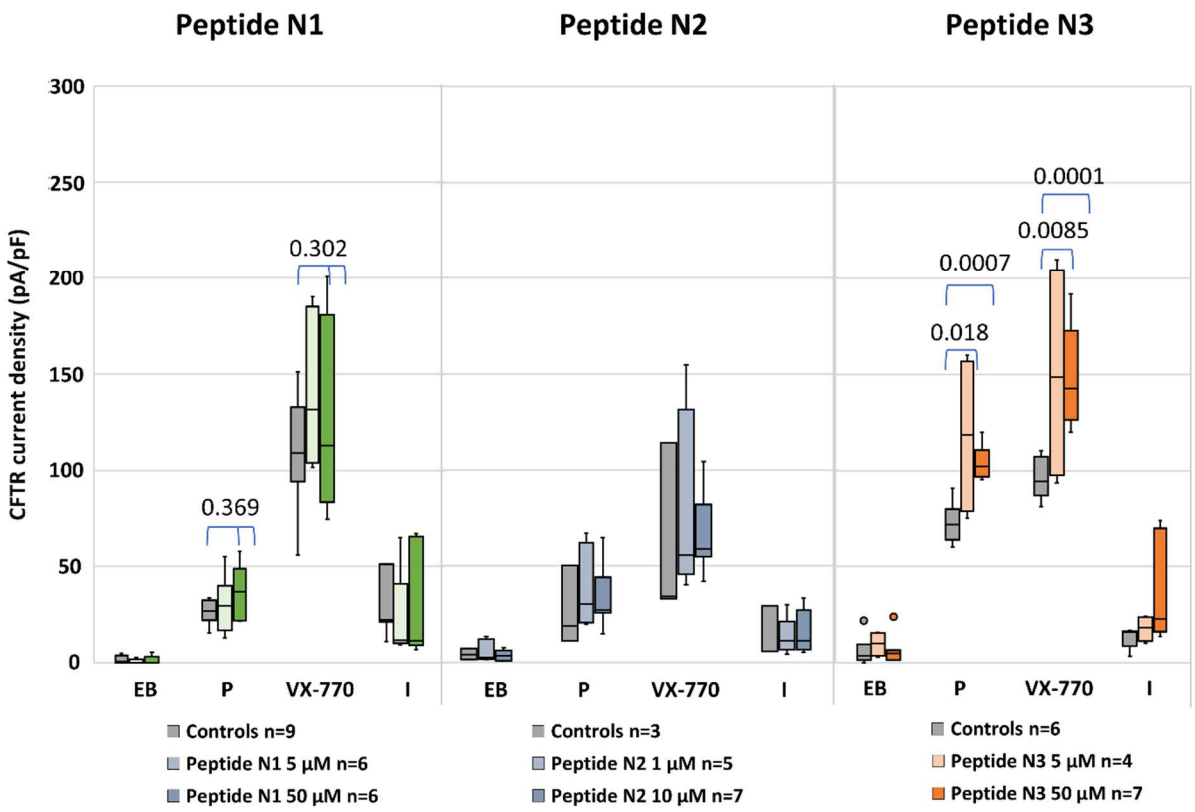


**Figure 6. Functional evaluation of Series II peptides N1, N2 and N3 by aPC technology (QPatch).** Experimental values (mean SEM) obtained after addition of 5 or 50 µM of N1, N2 or N3 peptides. Four conditions were applied to each cell: basal (extracellular buffer; EB), phosphorylation of CFTR channel stimulated by a forskolin and IBMX cocktail (P), condition P supplemented with VX-770 (VX-770) and inhibition of CFTR current by $inh_{172}$ and glibenclamide compounds (I). Statistical analyses were not done for the N2 peptide because of the small number of controls (no qualitative change compared to the N3 peptide results). P-values are shown underlined with blue horizontal brackets.

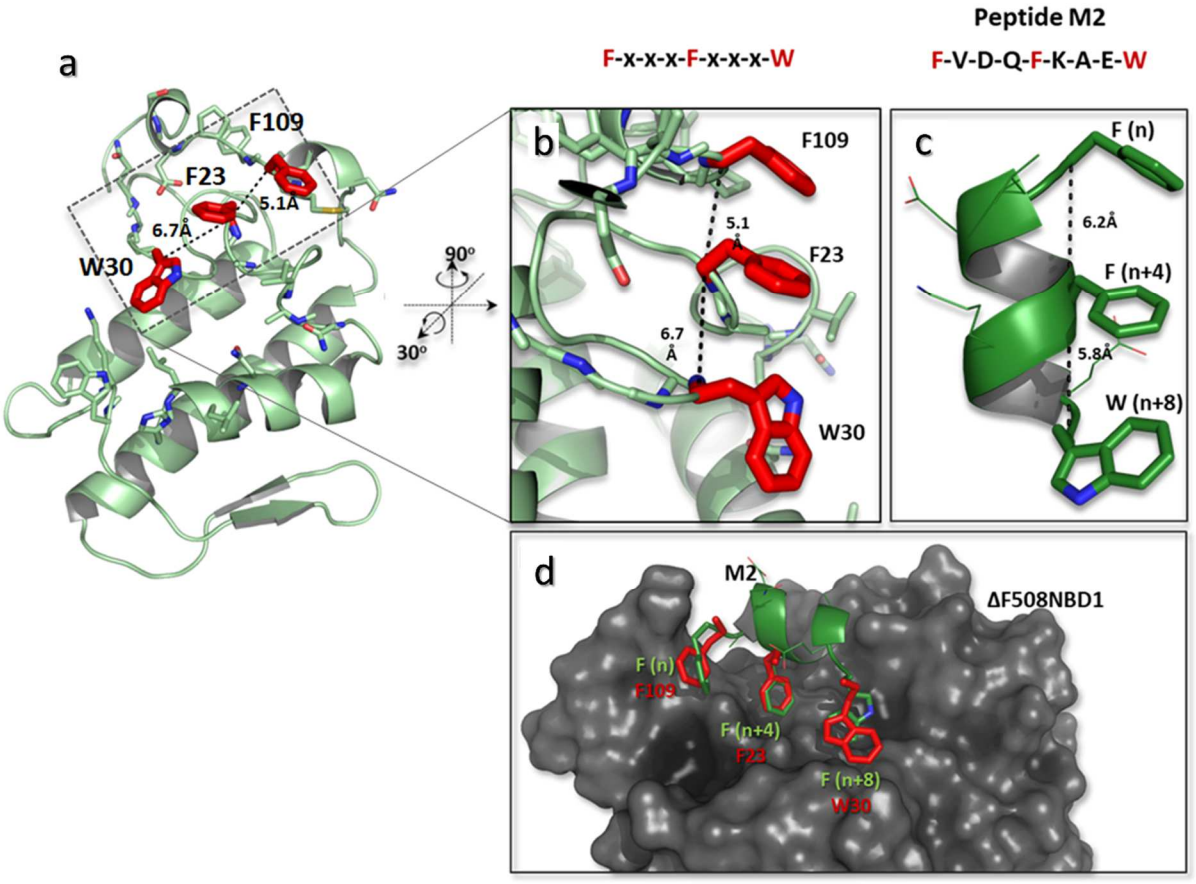


**Figure 7. Series III peptide M2 containing the hydrophobic motif FxxxFxxxW.** (a) The three hydrophobic residues W30, F23, F109 on the CBb interaction interface important for binding to ΔF508NBD1 and (b/c) comparison of their spatial arrangement with motif FxxxFxxxW on peptide M2 modeled as an α-helix. (d) Superimposed structures of peptide M2 and hydrophobic residues of CBb present on the surface of ΔF508NBD1.

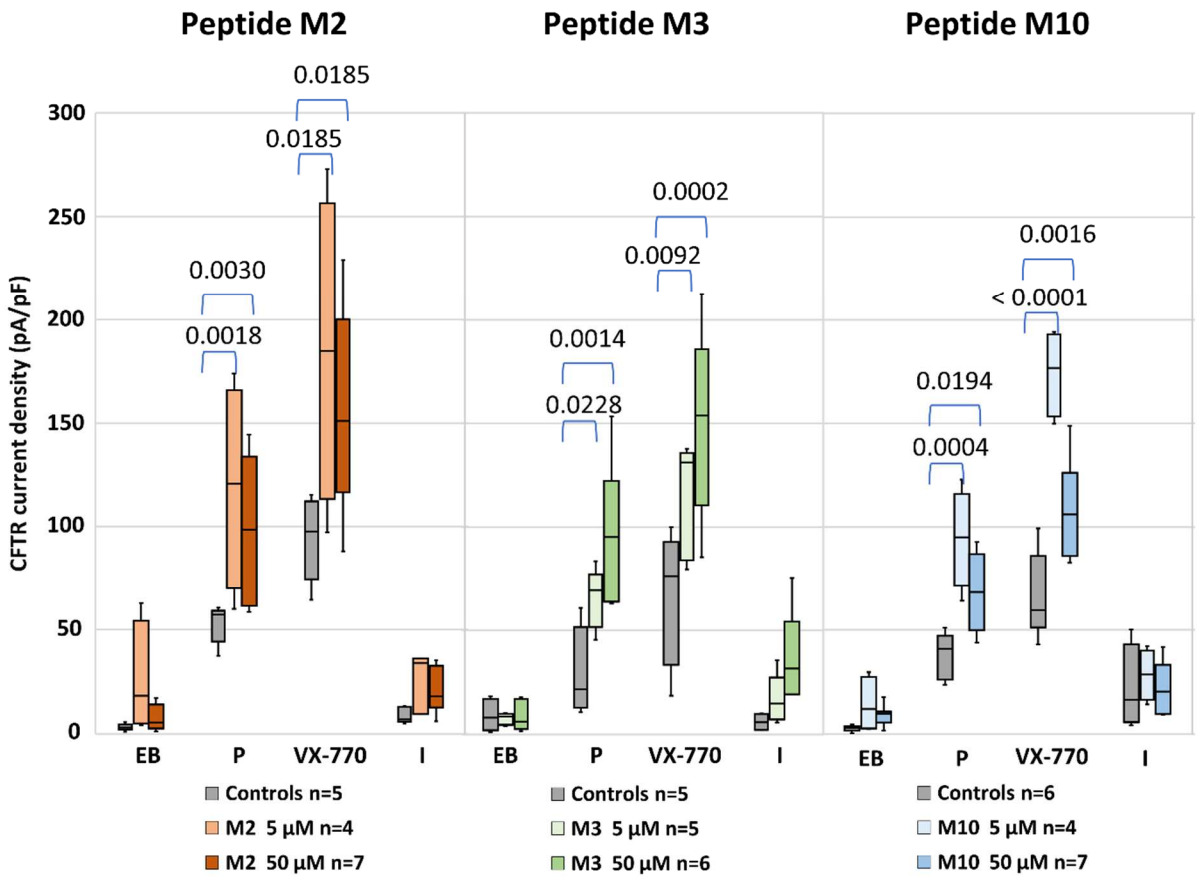


**Figure 8. Functional evaluation of Series III peptides M2, M3 and M10, by aPC technology (QPatch).** Experimental values (mean, SEM) obtained after addition of 5 or 50 µM of M2, M3 or M10 peptides. Four conditions were applied to each cell: basal (extracellular buffer; EB), phosphorylation of CFTR channel stimulated by a forskolin and IBMX cocktail (P), condition P supplemented with VX-770 and inhibition of CFTR current by Inh172 and glibenclamide compounds (I). P-values are shown underlined with blue horizontal brackets.

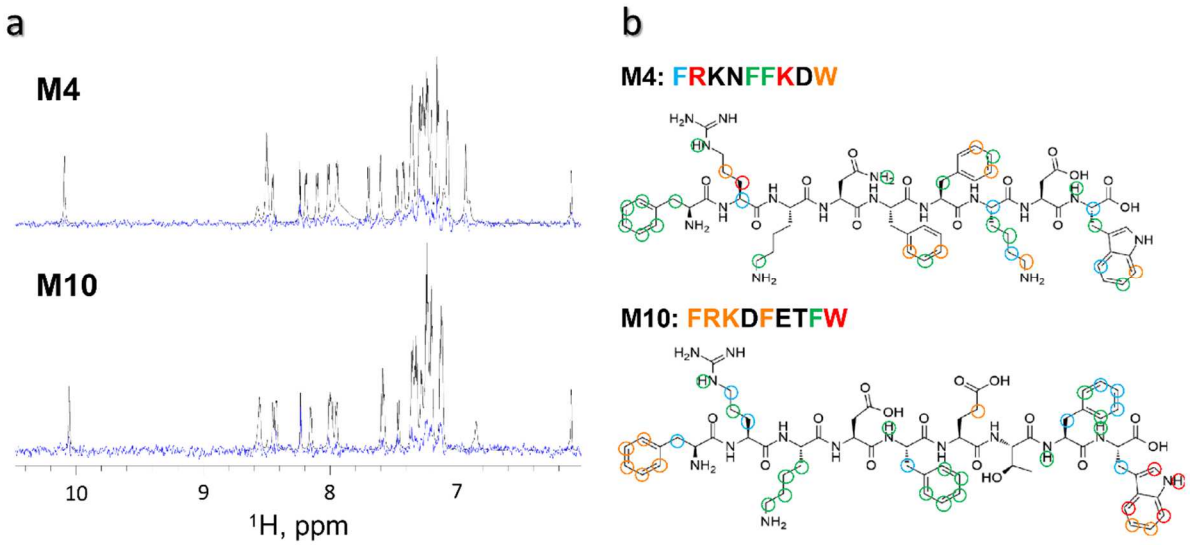


**Figure 9. Series III peptides M4 and M10 epitope mapping by NMR STD experiments**. (a) Low-field regions showing the 1D $^{1}$H signals of the amide and aromatic hydrogens of the peptides (1 mM, black) in the presence of ΔF508NBD1 (30 µM) and the corresponding corrected STD (cSTD) signals (blue). The corrected STD spectra were magnified 38x with respect to their original relative intensity. (b) The relative cSTD values for each hydrogen of the M4 and M10 peptides are represented by spheres of varying color. Red: very strong; orange: strong; green: medium; blue: weak. The name and sequence of the peptides are indicated; the relative importance of residues in binding was established from detailed inspection of the measured cSTD (**Table S6**). The sequences follow the same color-code as the spheres but takes into consideration signals' overlap and the other contacts in the residue.

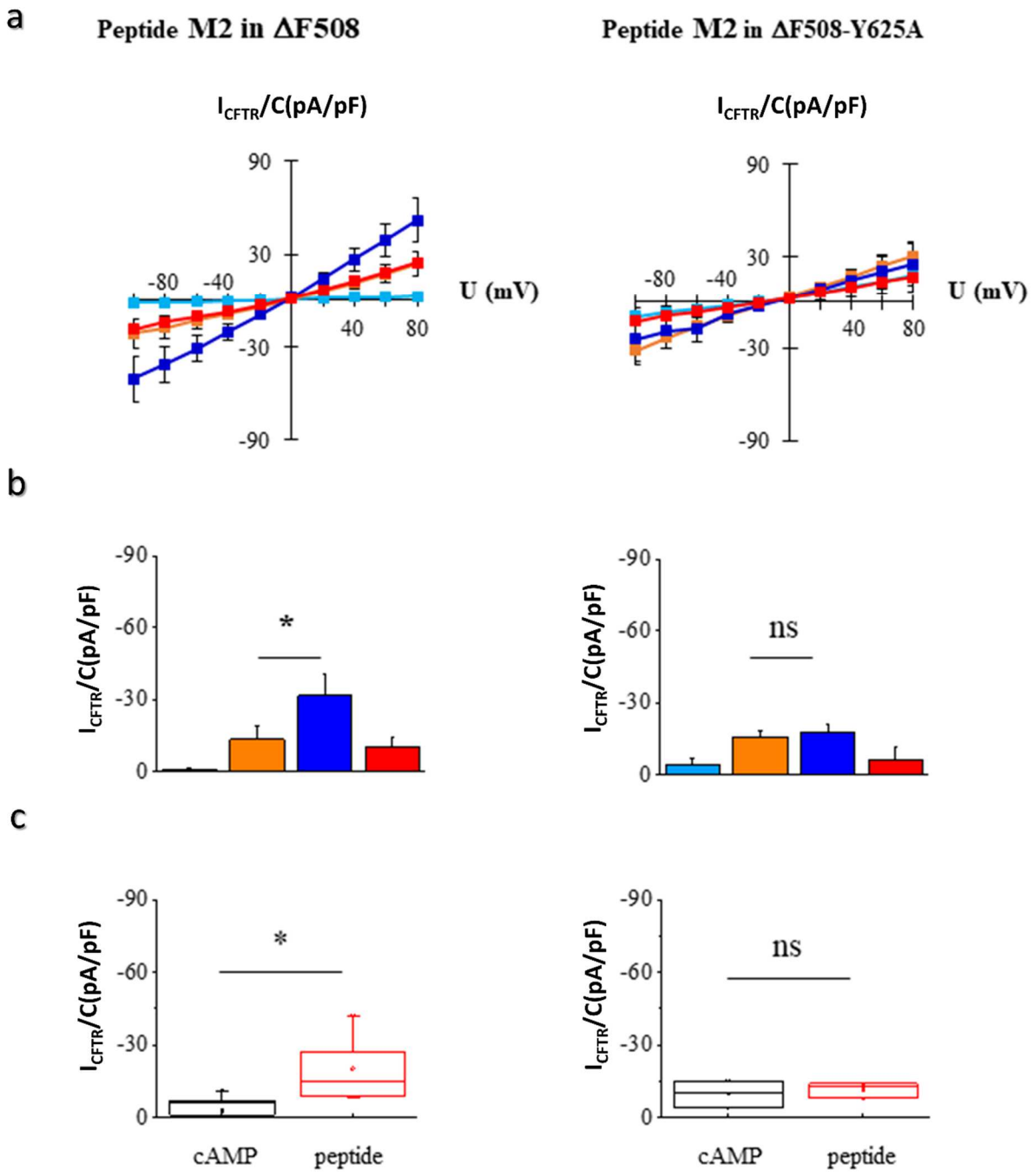


**Figure 10. Peptide M2 activity measured by whole-cell patch-clamp recordings in HEK293 cells expressing ΔF508CFTR or ΔF508-Y625ACFTR corrected by low temperature (27 °C).** (a) Mean (and SEM) current-voltage relationships recorded by holding the membrane potential at 0 mV and pulsing the voltage in the range from –100 mV to +80 mV at 20 mV steps: at basal level (light blue), after addition of 400 µM CPT-cAMP / 100 µM IBMX cocktail (orange), after addition of 1 µM peptide cocktail (dark blue) and inhibition by

5 μM $inh_{172}$/20 μM glibenclamide (red). (b) Current densities were normalized to cell capacitance (I/C). Peptide M2 (1 μM) with ΔF508CFTR or with ΔF508-Y625ACFTR (n=3). (c) Nonparametric tests (paired sample Sign tests) were performed between cAMP cocktail (black) and peptide M2 cocktail (red). At the significance level of 0.05, peptide M2 significantly increased cAMP-activated ΔF508CFTR currents (p=0.031, n=5) but not ΔF508-Y625ACFTR currents (n=3).

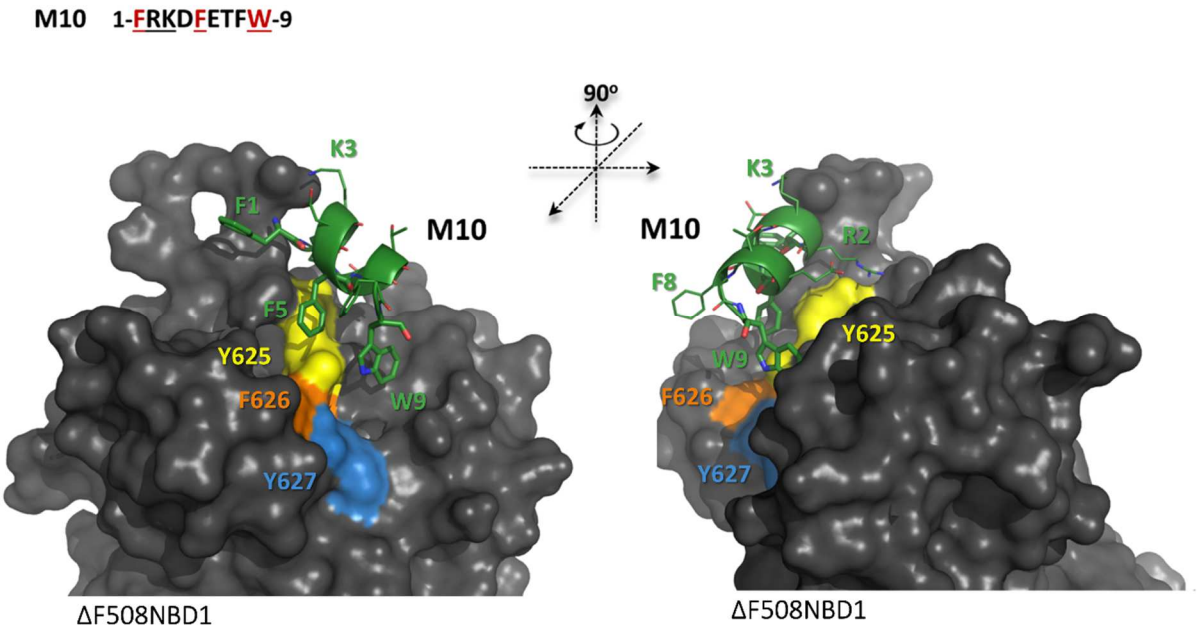


**Figure 11**. **Representative structure of the M10-ΔF508NBD1 complex from the best cluster obtained by molecular docking using HADDOCK**. The solvent accessible surface area of ΔF508NBD1 is shown in grey, and peptide M10 in green (ribbon and sticks for side chains). The hydrophobic residues Y625, F626 and Y627 on the ΔF508NBD1 surface are shown in yellow, orange and light-blue, respectively.

## Protein Interface

## Peptide Design

## ΔF508-CFTR Binding and Potentiating Effect